KVN Status Report 2024

Korean VLBI Network,
Korea Astronomy and Space Science Institute

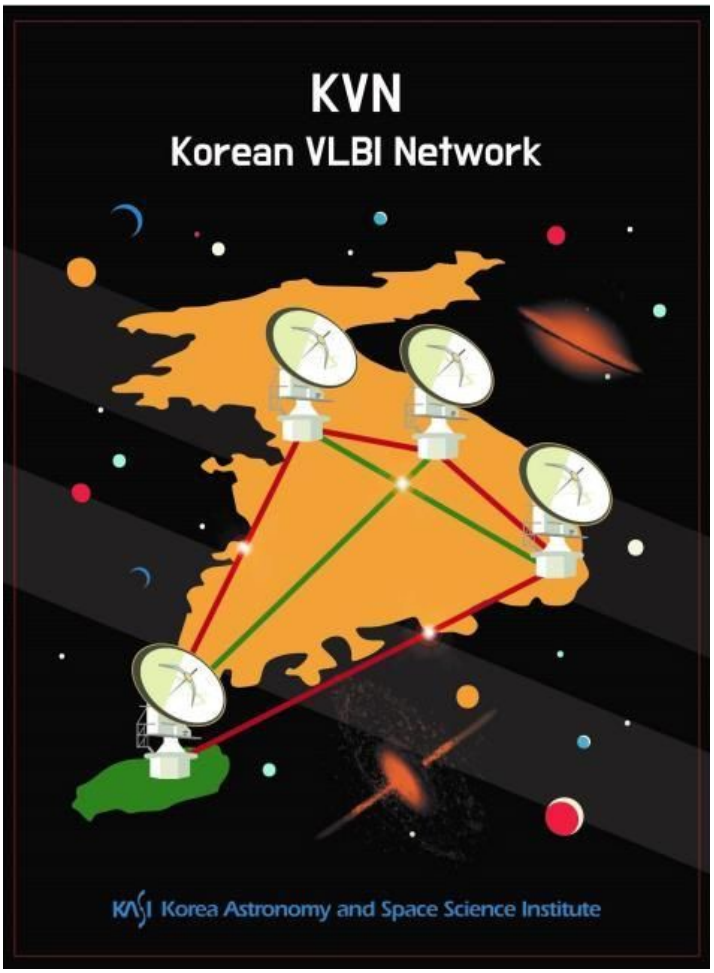

April 24, 2024
KVN group, Radio astronomy division

Contents

List of Tables

List of Figures

1 Introduction

The Korean VLBI Network (KVN) is the only Very Long Baseline Interferometry (VLBI) facility in Korea. It consists of four 21-m radio telescopes, located in Seoul (Yonsei University), Ulsan (University of Ulsan), Jeju, and Pyeongchang (newly constructed on the Pyeongchang campus of Seoul National University). This network offers a comparable spatial resolution to a radio telescope spanning about 500 km (see Figure 1). However, it is considered a relatively modest network when compared to the larger American and European VLBI networks, such as the Very Long Baseline Array (VLBA) and the European VLBI Network (EVN). To address this limitation, KASI has developed innovative multi-frequency band receiver systems that simultaneously observe four different frequencies: K, Q, W, and D bands (with center frequencies of 22, 43, 86, and 129 GHz). Additionally, the newly constructed Pyeongchang Telescope has extended its observing range to 230 GHz band. This remarkable capability enables the KVN to study the formation and evolutionary processes of stars, the structure and dynamics of our galaxy, the nature of active galactic nuclei, and more, with milli-arcsecond resolution [1]. By employing such advanced technology, we have demonstrated its commitment to pushing the boundaries of scientific research and fostering collaboration among experts in the field.

2 KVN System

2.1 Network

2.1.1 Array

The KVN is a four-component VLBI network in South Korea dedicated to millimeter-wavelength VLBI observations. Four 21-m radio telescopes are strategically positioned in Seoul, Ulsan, Jeju, and Pyeongchang, respectively: each is the KVN Yonsei Radio Telescope (hereafter KYS), the KVN Ulsan Radio Telescope (hereafter KUS), the KVN Tamna Radio Telescope (hereafter KTN), and the KVN Pyeongchang Radio Telescope (hereafter KPC). The baseline lengths of these telescopes span from 133 to 478 km. All these antennas share an identical design, ensuring uniformity in their capabilities and performance (see Figure 2).

2.1.2 UV coverage

Figure 3 presents the simulated UV coverage of the KVN at K-band for sources with varying declination (+60°, +30°, 0°, and −30°) observed over 12 hours.

2.1.3 Antenna location

Table 1 presents the coordinates of KVN antennas, while Table 2 shows the geometric locations of the four KVN stations. The position of all antennas has been determined using GPS, and KVN antenna positions are routinely monitored by GPS and geodetic VLBI observations in collaboration with VLBI Exploration of Radio Astrometry (VERA) of Japan.

Figure 1: The location of the Korean VLBI Network (KVN).

Table 1: The geographical locations of the KVN antennas

Antenna	Longitude (° ′ ″)	Latitude (° ′ ″)	Altitude (m)
KYS	126:56:27.4	37:33:54.9	139
KUS	129:14:59.3	35:32:44.2	170
KTN	126:27:34.4	33:17:20.9	452
KPC	128:26:55.1	37:32:00.1	557

2.1.4 Array Operation Center (AOC)

KVN antennas can be remotely controlled by the Array Operation Center (AOC) at the East Asia VLBI Center, KASI, Daejeon. KVN stations are interconnected with the AOC by a high-speed dedicated network called KREONET (Korea Research Environment

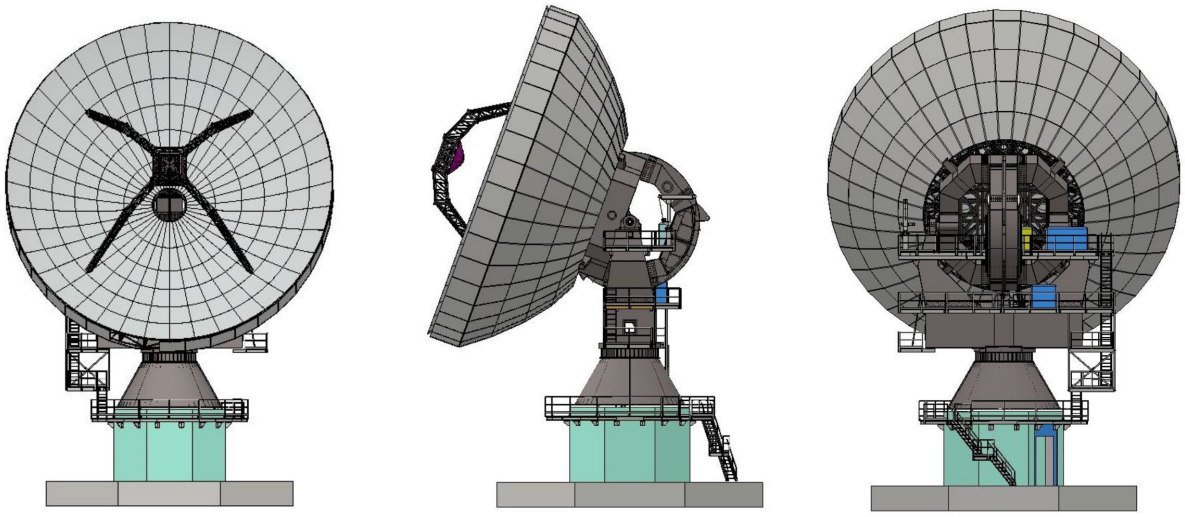

Figure 2: Design of the KVN antenna.

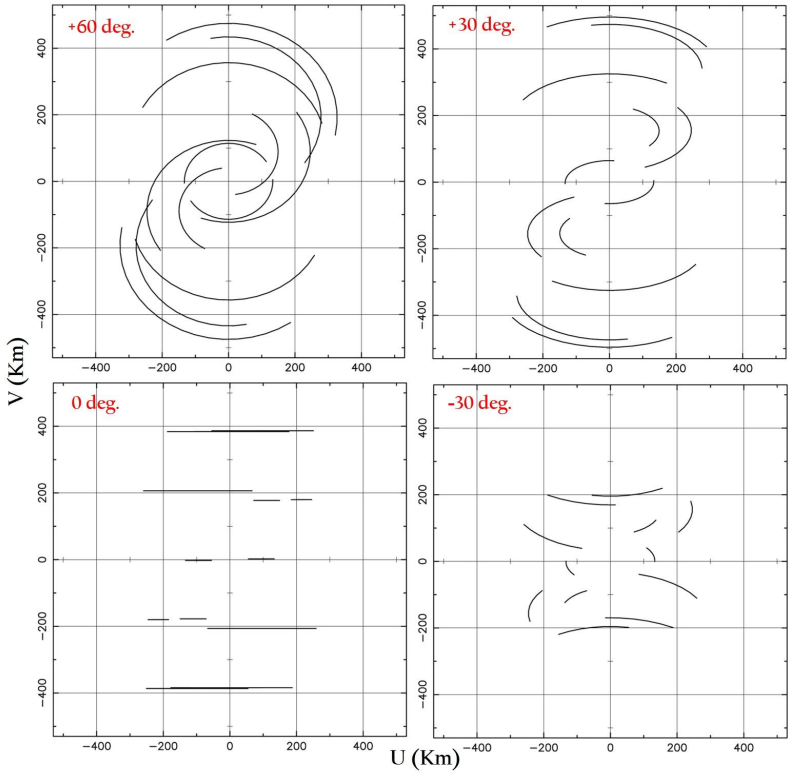

Figure 3: UV coverage simulation for the K-band.

Open NETwork). Considering the KVN antennas can be controlled remotely from the AOC, it is vital that the AOC operator is aware of the weather conditions that can influence the quality of the VLBI data. Each KVN observatory has its own weather station that transmits information on air temperature, dew point, wind speed, wind direction, and air pressure to the AOC.

Table 2: Positions of KVN antennas by IVP measurement using GNSS

Antenna	Epoch	X (m)	Y (m)	Z (m)
KYS	Sep. 20, 2019	−3042281.0290	4045902.6673	3867374.3313
KUS	Jun. 18, 2023	−3287268.8665	4023449.9997	3687379.9024
KTN	Nov. 19, 2022	−3171731.8636	4292678.3969	3481038.6857
KPC	Nov. 18, 2923	−3149228.7545	3966414.5854	3864840.1879

2.2 Antennas

2.2.1 Optics and Driving performance

The KVN antennas are shaped Cassegrain-type antennas featuring altitude-azimuth mounts. The main reflector has a diameter of 21-m and a focal length of 6.78-m. Comprising 200 aluminum panels, the main reflector achieves a manufacturing surface accuracy of approximately 65 μm. The main reflector can move at a speed of 3°/second, facilitating fast position-switching observations. The position, tilt and tip of the sub-reflector are remotely controlled and modelled to account for the effects of gravitational deformation on the main reflector and sagging of the sub-reflector. Furthermore, the newly constructed KPC antennas perform slightly better than the old KVN antennas. For further details on the antenna optics, kindly refer to Table 3.

Table 3: Specifications for KVN antenna optics

Main reflector (Axisymmetric Paraboloid)	Parameters
Diameter	D = 21.03 m
Focal length	f ≈ 6.78 m
Focal ratio	f/D = 0.32
Panels manufacturing accuracy	65 μm (KVN), ≤ 60 μm (KPC)
Alignment surface accuracy	54 μm (KVN), ≤ 50 μm (KPC)
Sub-reflector (Hyperboloid) diameter	**Parameters**
Diameter	d ≈ 2.25 m
Manufacturing surface accuracy	50 μm (KVN), ≤ 30 μm (KPC)
Expected total surface accuracy	124 μm at EL 48°
Slewing speed	3 °/sec
Slewing acceleration	3 °/sec^2
Operating range	Az.: −90° ∼ +450°, El.: 0° ∼ 90°

2.2.2 Gain Curve

The main reflector panels of KVN antennas were installed to give the maximum gain at the elevation angle of ∼ 48°. The sagging of the sub-reflector and the deformation of the main reflector by gravity with elevation results in degradation of antenna aperture efficiency

with elevation. To compensate for this effect, a hexapod is utilized to adjust the sub-reflector position in KVN antennas. Although the hexapod correction reduces significantly the dependence of aperture efficiency with elevation, the degradation still appears evidently at a higher frequency. By tracking strong maser sources or planets such as Jupiter or Mars at different altitudes, we can measure how the efficiency of the antenna changes relative to elevation. Figure 4 shows the elevation dependency of antenna gain of the KVN 21-m radio telescopes measured by observing several strong maser sources, Mars, Jupiter, and 3C 84, utilizing the observation mode of "Five pointing" and "Cross Scan". For the KPC, the D band receiver has not been installed yet, so no gain curve measurements have been conducted. Instead, a 230 GHz receiver was installed in 2023 for the performance test of the antenna, and the results are shown in Figure 5. However, the 230 GHz receiver has also been removed for now, and the receiver for the truly research observations will be installed in the second half of 2024.

We derived a normalized gain curve which has the following form: $G\_norm = A0 \cdot EL^2 + A1 \cdot EL + A2$, where EL is the elevation in degree, by fitting a second-order polynomial to the data and normalizing the fitted function with its maximum value. The fitted parameters are summarized in Table 4. The values displayed in Table 4 represent the average of Left Circular Polarization (LCP) and Right Circular Polarization (RCP).

Table 4: Coefficients of normalized gain curves (the average of LCP and RCP)

Station	Reference Freq.	A0	A1	A2
KYS	22	−8.9467E−06	5.4653E−04	9.9150E−01
	43	−2.4528E−05	1.4734E−03	9.7785E−01
	86	−5.6926E−05	4.7124E−03	9.0124E−01
	129	−1.5973E−04	1.3696E−02	7.0643E−01
KUS	22	−1.9115E−05	1.4894E−03	9.7040E−01
	43	−5.1311E−05	4.5593E−03	9.0199E−01
	86	−3.8227E−05	3.1453E−03	9.3526E−01
	129	−1.2589E−04	1.0413E−02	7.8466E−01
KTN	22	−1.0840E−05	9.6959E−04	9.7824E−01
	43	−1.6814E−05	1.7814E−03	9.5205E−01
	86	−5.6926E−05	4.7124E−03	9.0124E−01
	129	−1.1899E−04	1.2518E−02	7.4806E−01
KPC	22	−1.5632E−05	1.1750E−03	9.7792E−01
	43	−5.3563E−05	4.8118E−03	8.9193E−01
	86	−3.3422E−05	3.1433E−03	9.2609E−01
	150	...	...	...
	230 (test receiver)	−3.1383E−04	2.9651E−02	2.9958E−01

2.2.3 Antenna beam size and Aperture efficiency

Between December 2021 and March 2022, main reflector panel alignments (using photogrammetry) were carried out on three existing KVN antennas. In March 2024, an ad-

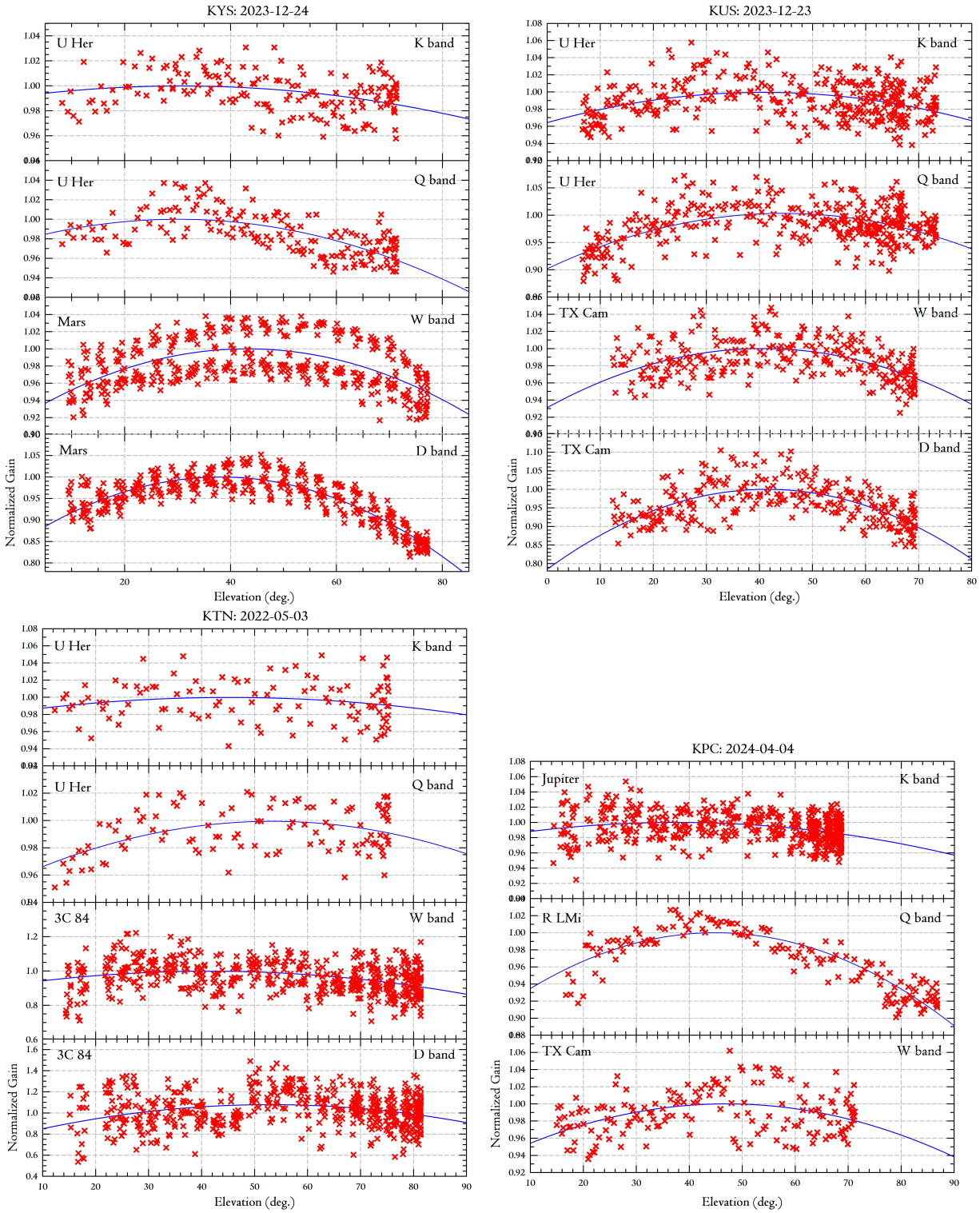

Figure 4: Normalized gain curves of four bands (22, 43, 86, 129 GHz) at each KVN antenna.

ditional panel alignment was performed on the KYS antenna, and the sub-reflector was replaced. Furthermore, the measurement of the primary mirror panels for the recently con-

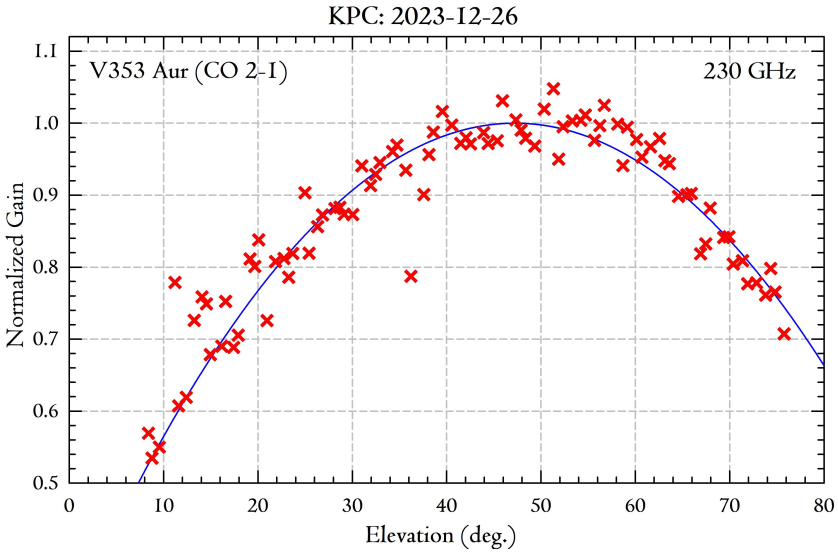

Figure 5: Normalized gain curves of 230 GHz (using test receiver) at the KPC.

structed KPC antenna was completed in March 2024. Accordingly, the surface accuracies of four KVN telescopes were enhanced to 52 (KYS), 72 (KUS), 70 (KTN), and 55 (KPC) μm, respectively. Furthermore, the KVN system was recently upgraded to a wide-band receiving system employing a new sampler, the OCTAD, encompassing the frequency ranges of 18–26 GHz (K), 35–50 GHz (Q), 85–116 GHz (W), and 125–142 GHz (D), respectively (see Section 2.3). Therefore, in all wide K, Q, W, and D bands, we measured HPBW, aperture efficiency, and main-beam efficiency using the OCTAD. However, the KPC has not yet been fully set up with OCTAD, so limited measurements have been made at K, Q, and W bands.

The results are shown in Table 5 as representative values for each band. While the W and D band values were acquired through observations toward Mars and Uranus, the K and Qband values were obtained through observations toward Jupiter. The brightness temperatures for Jupiter in the K and Q bands are applied from de Pater et al. (2019)[2] and Maris et al. (2021)[3]. The estimates for the W and D bands use the Mars brightness modeling data that are displayed on its website[1]. Figure 6 displays the efficiency and beam size for each band of the telescopes.

- **Elevation dependency**
  With elevation, aperture efficiency changes. The previous section provided the gain curve that depicts the elevation dependency of the KVN antennas. The maximum values are those listed in Column (4).

- **Frequency dependency of beam efficiency**
  Beam efficiency also varies with beam size. The measured HPBWs are tabulated in Column (3), which are almost the same as the theoretical one (= λ/D of the antenna). To get a beam efficiency at 90 GHz, you have to multiply $(86/90)^2$ to that at 86 GHz.

[1] https://lesia.obspm.fr/perso/emmanuel-lellouch/mars/

Table 5: Beam size, efficiencies, and DPFU[a] of each KVN antenna

Site	Frequency (Band) (GHz)	HPBW (arcsec)	η_A (%)	η_B (%)	DPFU (K/Jy)
(1)	(2)	(3)	(4)	(5)	(6)
KYS	22 (K)	130	65	56	0.0816
	40 (Q-low)	73	70	60	0.0876
	43 (Q-high)	66	67	56	0.0841
	47 (Q-high)	64	71	60	0.0887
	86 (W-low)	33	55	38	0.0690
	95 (W-low)	30	46	38	0.0572
	103 (W-high)	28	46	39	0.0582
	111 (W-high)	27	46	40	0.0572
	129 (D)	27	32	32	0.0404
	140 (D)	24	31	35	0.0387
KUS	22 (K)	127	71	58	0.0885
	40 (Q-low)	72	68	58	0.0855
	43 (Q-high)	66	68	56	0.0852
	47 (Q-high)	61	66	57	0.0833
	86 (W-low)	32	48	38	0.0607
	95 (W-low)	29	58	45	0.0723
	103 (W-high)	27	56	45	0.0698
	111 (W-high)	26	55	47	0.0685
	129 (D)	23	40	34	0.0500
	140 (D)	21	42	38	0.0521
KTN	22 (K)	128	71	59	0.0891
	40 (Q-low)	69	59	47	0.0745
	43 (Q-high)	63	67	50	0.0843
	47 (Q-high)	59	56	45	0.0705
	86 (W-low)	34	58	50	0.0722
	95 (W-low)	29	53	43	0.0666
	103 (W-high)	28	51	43	0.0645
	111 (W-high)	27	44	40	0.0548
	129 (D)	22	34	29	0.0430
	140 (D)	22	33	32	0.0417
KPC	22 (K)	123	75	62	0.0942
	47 (Q)	59	73	59	0.0921
	90 (W)	32	67	56	0.0834

[a] indicates the Degree Per Flux density Unit.
η_A: Aperture efficiency, η_B: Main-beam efficiency.

- **Quantization correction of single-dish spectrum data**
  Prior to performing efficiency adaptations, single-dish spectrum data must be multi-

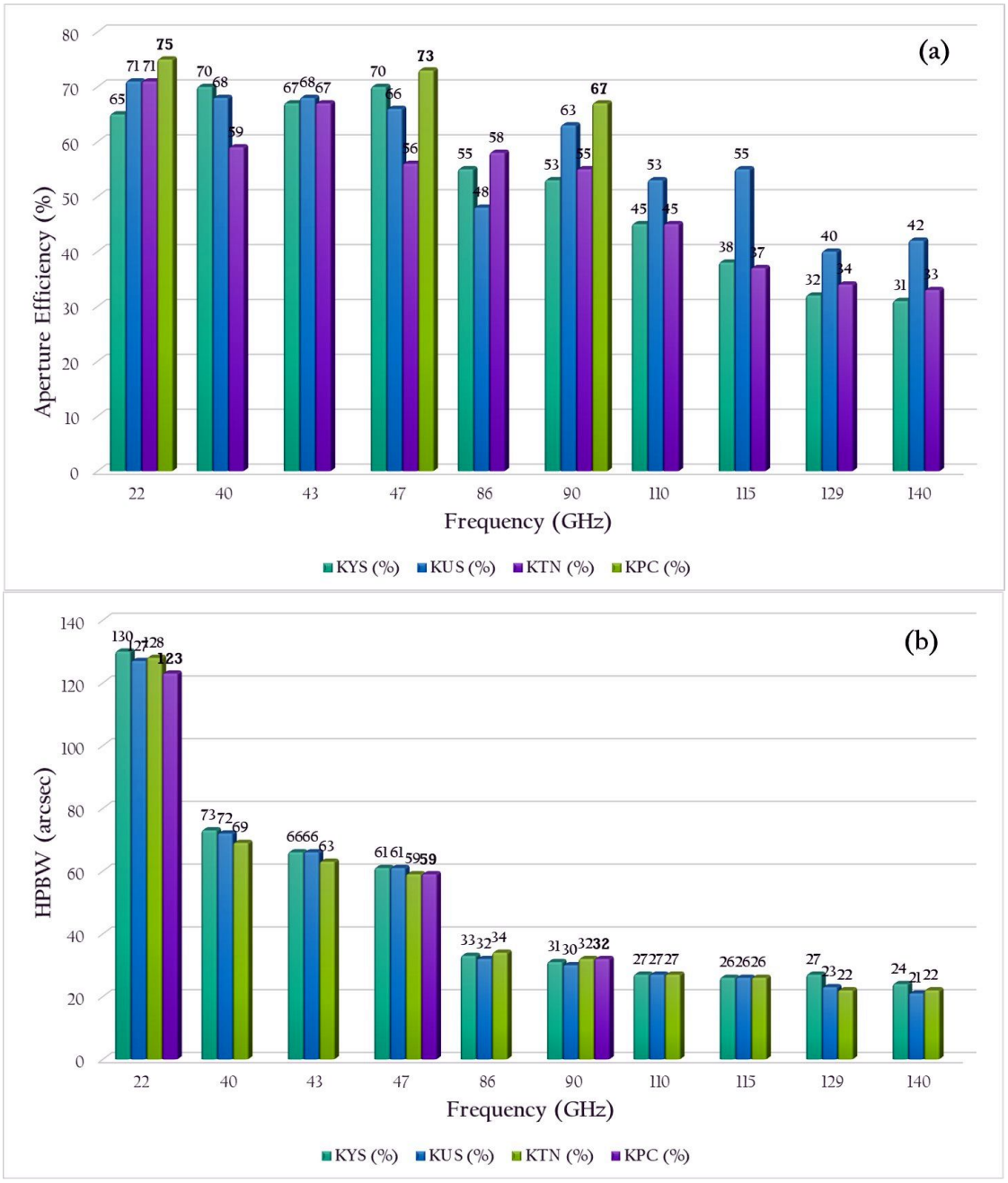

Figure 6: Aperture efficiencies and HPBWs of four KVN telescopes. (a): Aperture efficiency, (b) HPBW.

plied by a factor of 1.25 if it is being reduced. This is to compensate for the effects of the digital filter and spectrometer.

- Parameters of Table 5 can be applied for the following observing season;
  - KYS: from March 2024 – now
  - KUS: from December 2023 – now

– KTN: from December 2023 – now

– KPC: from April 2024 – now

2.2.4 Beam pattern

The KVN antenna optics are of the shaped-Cassegrain type, with a main reflector and sub-reflector designed to provide uniform illumination on an aperture plane. This design allows for greater aperture efficiency compared to conventional Cassegrain-type antennas. However, it should be noted that it also results in a higher sidelobe level, which may need to be taken into consideration. Figure 7 displays On-The-Fly (OTF) images of Venus and Jupiter at 86 GHz and 129 GHz, and 22 GHz and 43 GHz, respectively, as measured using the KYS antenna. The map size is $12' \times 10'$ for 22 and 43 GHz, and $3.5' \times 3'$ for 86 and 129 GHz. The first sidelobe pattern is visible. It is worth noting that KVN antennas typically exhibit sidelobe levels of -14 to -13 dB.

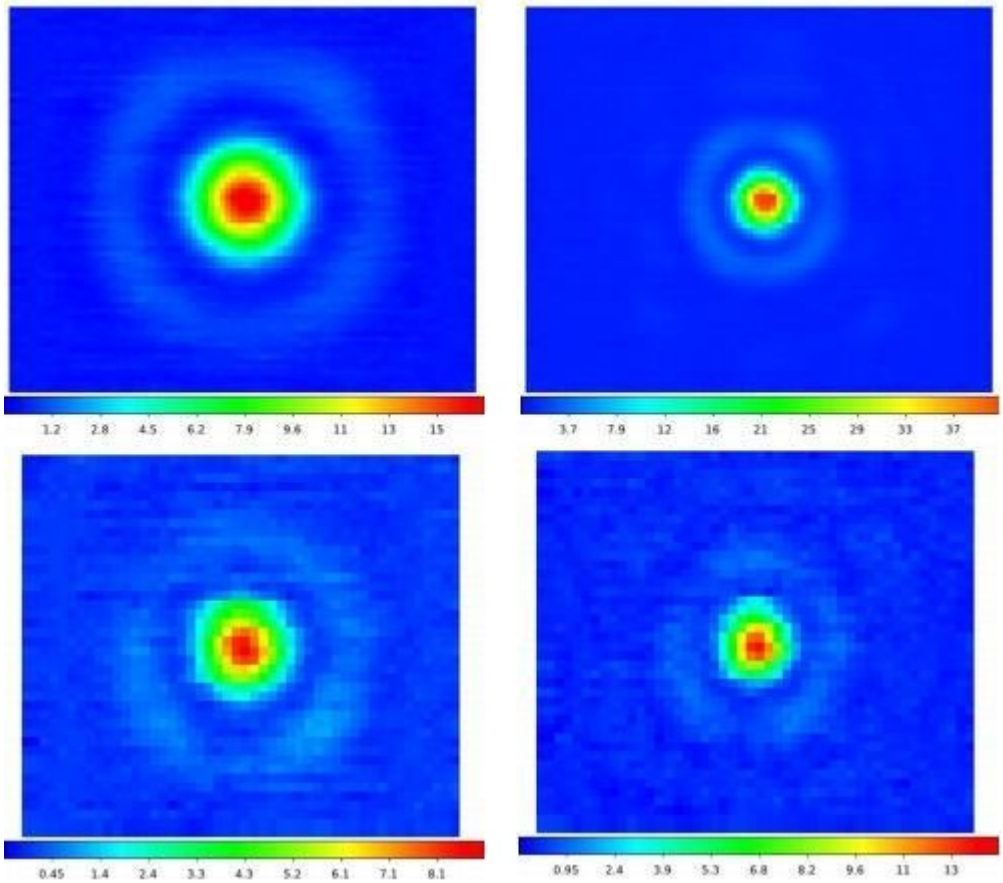

Figure 7: Beam patterns at the KYS antenna. Top panels: Jupiter at 22 GHz (left) and 43 GHz (right), Bottom panels: Venus at 86 GHz (left) and 129 GHz (right).

2.2.5 Antenna pointing accuracy

There can be systematic differences between the direction a radio telescope is intended to point and the direction it actually points. These differences can be caused by factors such as errors resulting from the telescope axis not being aligned with the true altitude-azimuth axis, deviations due to warped bearing planes, deviations due to gravitational deformation, and deviations due to non-ideal telescope construction. These systematic and recurring orientation errors are often expressed as a function of altitude and azimuth. The pointing model offers values for these errors based on altitude and azimuth to make necessary adjustments.

The KVN antenna aims for an accuracy of 4 arcseconds. In order to achieve and sustain this level of precision, periodic observations are taken to construct a pointing model. The equations of the pointing model for the KVN are given below:

$$\begin{aligned}\Delta\mathrm{A} &= \mathrm{IA} + \mathrm{CA}\ \sec(\mathrm{E}) + \mathrm{NPAE}\ \tan(\mathrm{E}) + \mathrm{AN}\ \tan(\mathrm{E})\ \sin(\mathrm{A}) - \mathrm{AW}\ \tan(\mathrm{E})\ \cos(\mathrm{A}) \\ &\quad + \mathrm{WA1}\ \tan(\mathrm{E})\ \sin(2\mathrm{A}) + \mathrm{WA2}\ \tan(\mathrm{E})\ \cos(2\mathrm{A}) + \mathrm{Aobs}\ \sec(\mathrm{E}) \\ \Delta\mathrm{E} &= \mathrm{IE} + \mathrm{GF}\ \cos(\mathrm{E}) + \mathrm{GF2}\ \sin(\mathrm{E}) + \mathrm{AN}\ \cos(\mathrm{A}) + \mathrm{AW}\ \sin(\mathrm{A}) + \mathrm{WA1}\ \cos(2\mathrm{A}) \\ &\quad + \mathrm{WA2}\ \sin(2\mathrm{A}) + \mathrm{R(Ps, Ts, RH, E)} + \mathrm{ERC}\ \cot(\mathrm{E}) + \mathrm{Eobs}\end{aligned}$$

In the above equation, IA = Az encoder zero offset, CA = Collimation error of RF axis, NPAE = Non-perpendicularity between Az & El axes, AN = Az axis misalignment in N-S, AW = Az axis misalignment in E-W, WA1 & WA2 = Azimuth bearing warp, Aobs = Az pointing offset, IE = El encoder zero offset, GF = Gravitational flexure correction at horizon, GF2 = Gravitational flexure correction for mis-centered EL drive and encoder system, ERC = Empirical correction for atmospheric refraction, Elobs = El pointing offset, and R(Ps,Ts,RH,E) = Refractive index of the atmosphere, where Ps, Ts, and RH = barometric pressure, temperature, and relative humidity, respectively.

Another factor that affects pointing accuracy is the impact of temperature differences in the antenna structure. This factor is challenging to incorporate into a basic pointing model due to its complex nature, which is influenced by variables such as the variance between the sun and antenna orientation, temperature differentials, and other factors. It is known that the temperature difference between the antenna yoke and pedestal has a significant effect on the pointing of the antenna. KVN has designed the antenna in a way that ensures the temperature difference between these parts is maintained below 1 degree (KVN-21M Technical Memo 136, 152). However, actual measurements have shown that the pointing is off by up to 10 seconds per hour during the day when the sun is shining. Therefore, it is necessary to make pointing observations at least every 2 hours during the day, especially at sunrise and sunset, in order to maintain the pointing accuracy at less than 6 arcseconds root mean square.

Since 2009, the telescope's pointing accuracy has been measured using a sample of evolved stars (mainly, 43 GHz SiO maser line). Table 6 presents the pointing accuracy of the four KVN telescopes that were observed in December 2023 and April 2024. In particular, we conducted pointing model observations at 86 GHz for the recently constructed KPC. Table 6 provides the total, azimuth, and elevation of the root mean square (rms) of the residual pointing offsets between the observations and the pointing models for each epoch and tele-

scope, accordingly ($Total\,Error = Sqrt(Az\_Error^2 + El\_Error^2)$). Figure 8 displays the residuals of each KVN telescope's pointing model.

Table 6: KVN Antenna Pointing Accuracy

Site	Total (arcsec)	Azimuth (arcsec)	Elevation (arcsec)	Frequency (GHz)	Date
KYS	**3.82**	1.92	3.30	43	December 10, 2023
KUS	**3.12**	1.19	2.88	43	December 10, 2023
KTN	**3.20**	2.17	2.35	43	December 16, 2023
KPC	**3.33**	2.24	2.46	86	April 06, 2024

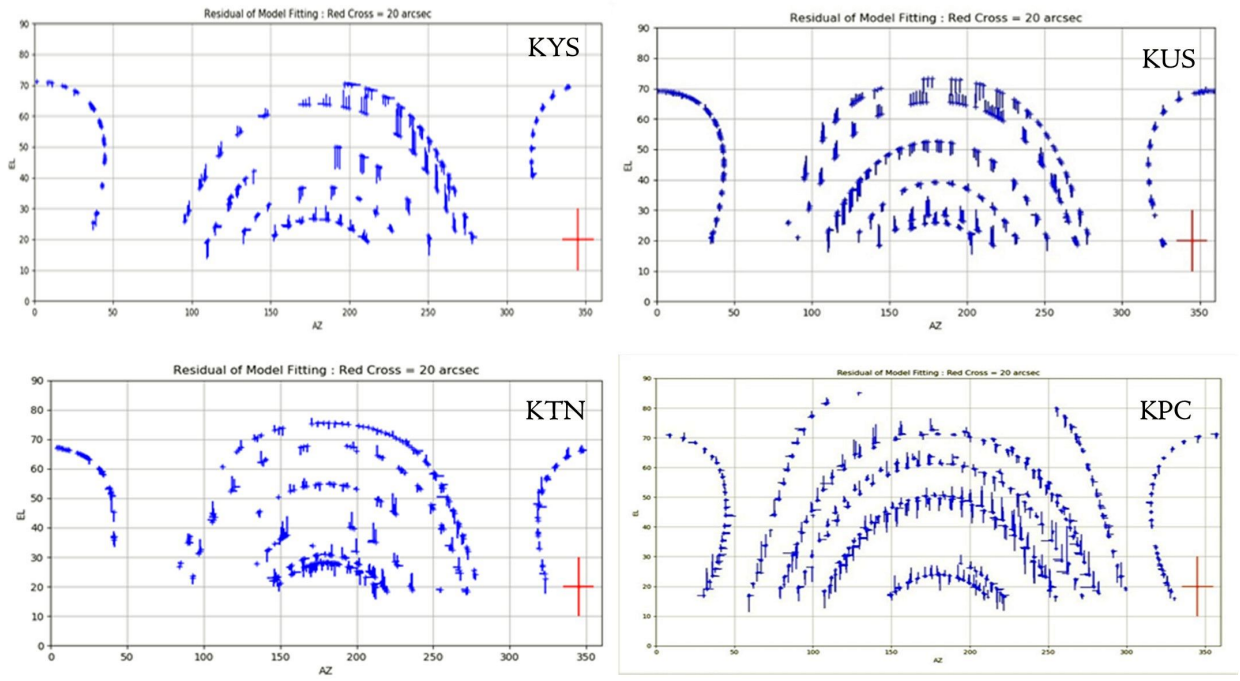

Figure 8: The residual of pointing models (KYS, KUS, KTN, and KPC from top-left to bottom-right).

2.2.6 Beam alignment

The quasi-optics should be set up for simultaneous observations of the four frequency bands such that each of the four beams is directed towards the same point in the sky. The other frequency bands' pointing offsets from the 86 GHz RCP beam's center are summarized in Table 7. After alignment, the cross-scan results were used to calculate the relative offsets. In contrast to the receiver systems utilized in previous KVN telescopes, the KPC is equipped with a Compact Triple-band Receiver (CTR), and currently, only LCP beams at 22, 43, and 86 GHz are available. Therefore, the 22 GHz and 43 GHz beams have been aligned with the 86 GHz LCP beam for the KPC.

Table 7: AZ/EL beam offset with respect to the 86 GHz RCP beam

Site	Band (L, R) (GHz)	Az. offset (arcsec)	El. offset (arcsec)	Measeured Date
KYS	22 (L)	+0.2 (±0.1)	+2.2 (±0.1)	February 02, 2024
	22 (R)	+1.0 (±0.2)	+1.9 (±0.2)	February 02, 2024
	43 (L)	+1.2 (±0.3)	+0.8 (±0.2)	February 02, 2024
	43 (R)	+2.9 (±0.4)	+0.8 (±0.3)	February 02, 2024
	86 (L)	−1.1 (±0.0)	−0.2 (±0.1)	February 02, 2024
	86 (R)			February 02, 2024
	129 (L)	+1.0 (±0.4)	−3.4 (±0.6)	February 02, 2024
	129 (R)	+2.4 (±0.7)	−3.2 (±0.6)	February 02, 2024
KUS	22 (L)	−0.8 (±0.5)	+2.0 (±0.6)	September 30, 2021
	22 (R)	−1.6 (±1.4)	+3.1 (±0.1)	September 30, 2021
	43 (L)	−0.5 (±0.2)	+0.4 (±0.1)	September 30, 2021
	43 (R)	−1.0 (±0.0)	+0.3 (±0.0)	September 30, 2021
	86 (L)	−1.4 (±0.1)	−0.1 (±0.1)	September 30, 2021
	86 (R)			September 30, 2021
	129 (L)	−1.0 (±0.2)	+1.5 (±0.3)	September 30, 2021
	129 (R)	−1.3 (±0.1)	+1.1 (±0.4)	September 30, 2021
KTN	22 (L)	−2.6	+0.8	May 28, 2020
	22 (R)	−3.6	−0.1	May 28, 2020
	43 (L)	+0.3	−2.5	May 28, 2020
	43 (R)	+0.1	−1.8	May 28, 2020
	86 (L)			May 28, 2020
	86 (R)	+2.1	0.0	May 28, 2020
	129 (L)	+2.0	−1.2	May 28, 2020
	129 (R)	+0.8	−1.4	May 28, 2020
KPC	22 (L)	+0.3 (±0.2)	+1.3 (±0.2)	April 02, 2024
	43 (L)	+1.5 (±0.2)	−0.1 (±0.2)	April 02, 2024
	86 (L)			April 02, 2024

2.2.7 Skylines

Skylines are the limits of the viewable height with azimuth below which we cannot see the sky. These limits are determined by obstructions caused by the neighboring buildings, trees, and mountains. Skylines of KVN sites measured in 2014 are shown in Figure 9. In addition, the skyline of the KPC was measured in August 2019.

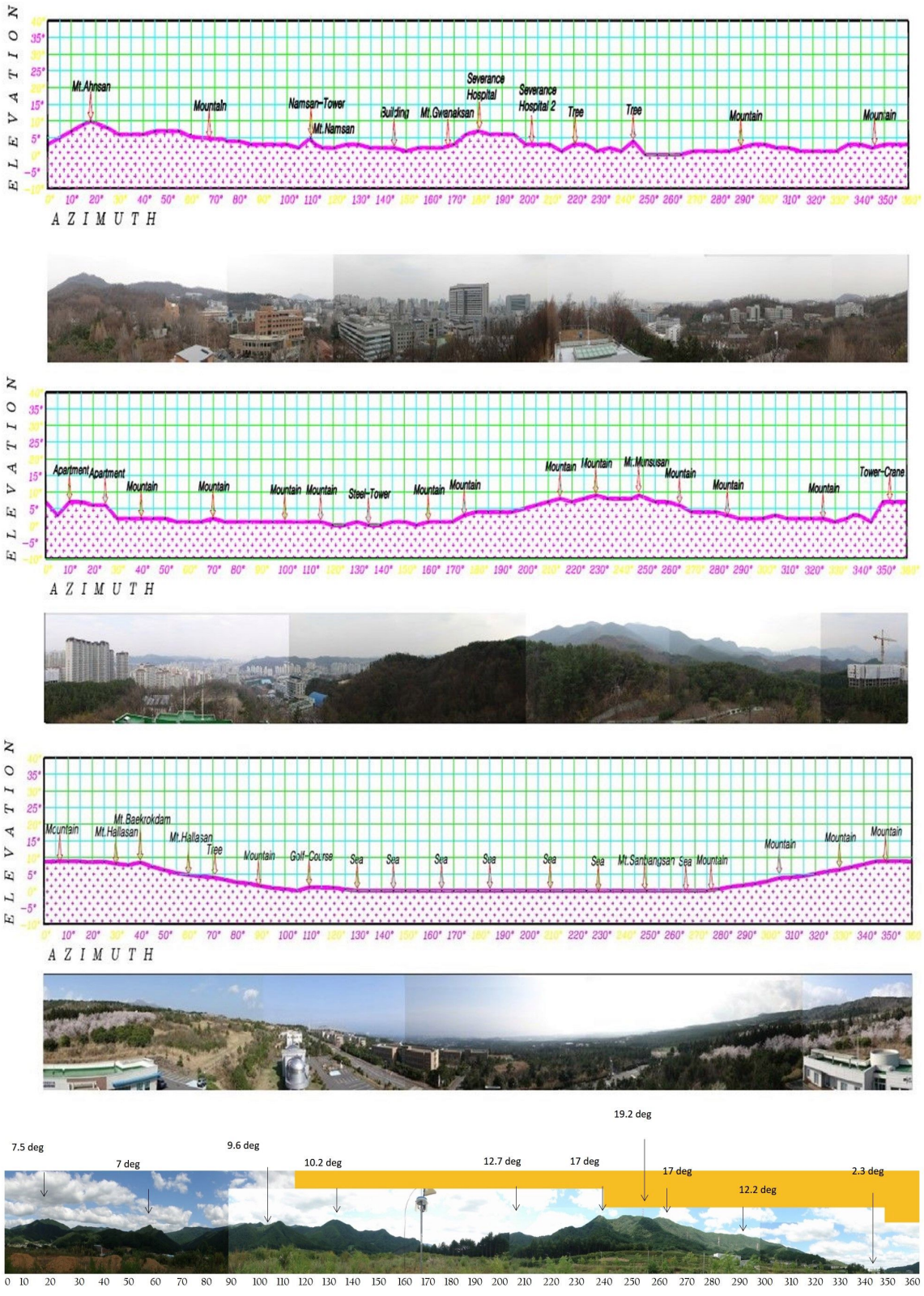

Figure 9: Skylines of KYS, KUS, KTN, and KPC from top to bottom.

2.3 Receiver

2.3.1 Quasi-optics

The KVN has the unique capability to observe four frequency bands [4], [5], simultaneously. KVN quasi-optics were designed to enable this multi-frequency observation. Figure 10 shows the layout of quasi-optics and receivers viewing from the sub-reflector side. The quasi-optics system splits one signal from the sub-reflector into four using three dichroic low-pass filters marked as LPF1, LPF2, and LPF3 in Figure 10. The split signals into four different frequency bands are guided to corresponding receivers.

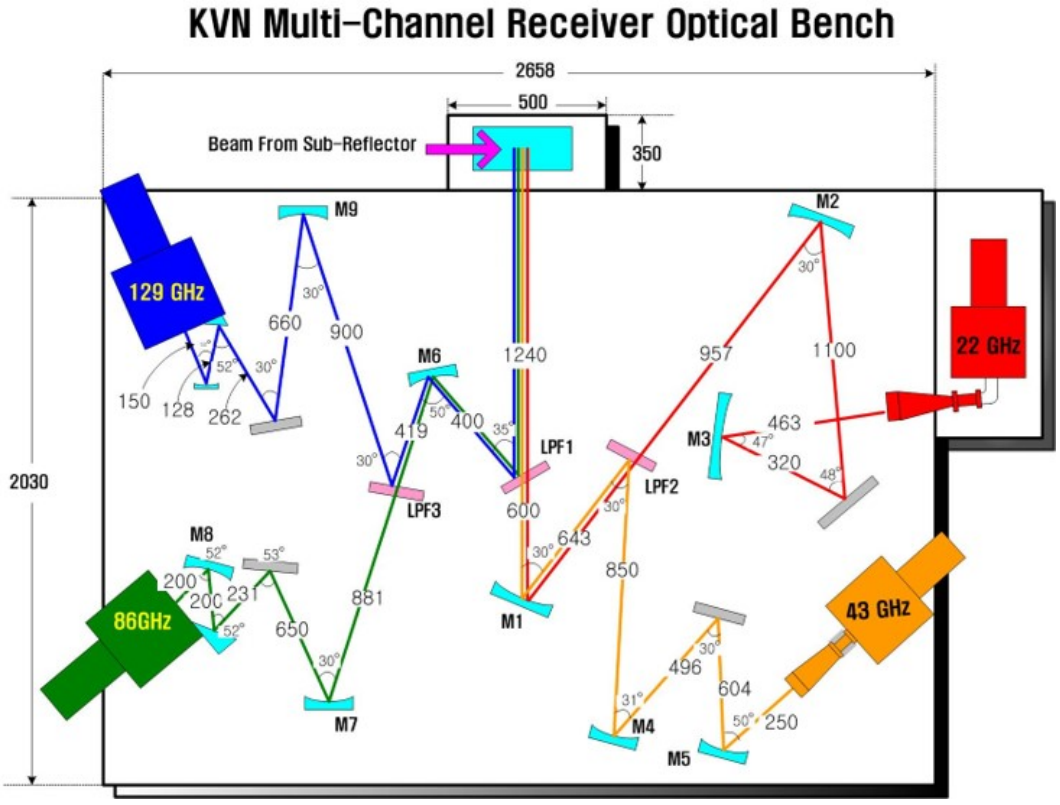

Figure 10: KVN multi-frequency receiving system.

In mid-2023, the construction of the KPC was completed. It has been conducting test observations until recently, with most of the testing finished. The receiving system of the KPC has been developed as an compact and wide-band receiver capable of simultaneous observations in the 18−230 GHz band. For the K, Q, and W bands, a compact three-channel receiver (a.k.a., CTR, Compact Triple-band Receiver) was designed and manufactured in-house to simultaneously observe them. To be more specific, the CTR system is mainly composed of a quasi-optical circuit, a cryogenic receiver, and a room temperature receiver system. The receiving frequency bands are divided into K (18–26 GHz), Q (35–50 GHz), and W band (80–116 GHz). These RF signals are then amplified and down-converted in the room temperature receiver, and finally converted into IF signals of 8–16 GHz. Additionally, it is possible to observe two polarization components (LCP and RCP) for each band simultaneously.

The quasi-optical circuit is a critical component that allows for simultaneous three-channel observations. It determines the antenna efficiency and receiver noise temperature, requiring complex design and high-quality assembly. Additionally, it necessitates sophisticated receiving beam alignment and precise measurement techniques. Cryogenic receiving systems are designed with a chamber that maintains a high vacuum and cryogenic temperature below 20 K. The chamber is equipped with a feed system that includes a cryogenic Low Noise Amplifier (LNA), feed horn, phase shifter, and orthogonal mode transducer (OMT). These components play a crucial role in influencing the receiver's noise temperature and stability. The room temperature receiving system comprises a room temperature amplifier and a local oscillator (LO) that convert the received RF signal to an intermediate frequency (IF). It also includes several band pass filters (BPFs), power divider, and mixers.

The production of the 150/230 GHz receiver and the C/X/Ka band receiver is currently underway.

Figure 11 illustrates that the configuration of the K/Q/W band CTR installed in the receiver room of the KPC and the additional receivers that will be installed.

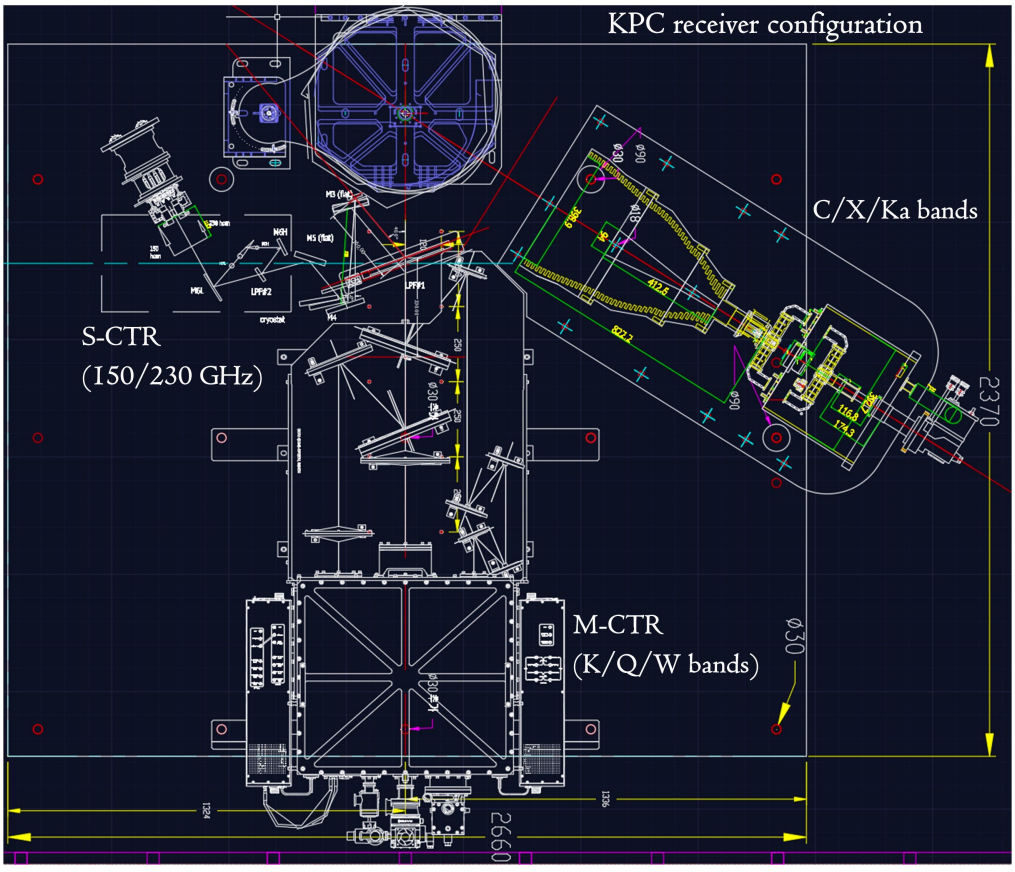

Figure 11: Layout of the CTR receiving system of the KPC.

2.3.2 Block diagram

The K, Q, and W-band receivers are cooled HEMT receivers, while the D-band receiver is an SIS mixer receiver [5]. All receivers are capable of receiving dual circular-polarization signals. Among eight signals (four dual-polarization signals), four signals selected by the IF selector are down-converted to the input frequency band of the sampler. The samplers digitize signals into 2-bit data streams with four quantization levels. The sampling rate is 1024 Mega samples per second, resulting in a 2 Gbps data rate (2-bit $\times$ 1024 megabytes per second) and 512 MHz frequency bandwidth. In total, we can get 4 streams of 512 MHz bandwidth (2 Gbps data rate) simultaneously, which means that the total rate is 8 Gbps.

New wide-band VLBI backends, including OCTAD, Mark 6, and GPU spectrometers, were installed for wide-band operation. They are indicated in the red box of Figure 12. The OCTAD consists of four analog-to-digital converters, digital signal processing modules, and a VDIF formatter. It digitizes four IF signals and performs signal processing for digital down-conversion and filtering. Combining OCTAD and ADS1K+Fila10G, all eight IF signals (four dual-polarization signals) can be obtained at the same time. The OCTAD has four 10 GbE outputs, with which we can get a maximum 32 Gbps aggregated data rate.

Furthermore, two wide-band VLBI sampler OCTADs were installed at KPC withe the objective of achieving enhanced performance in comparison to the original KVN system. As a result, the output rate of the KPC OCTAD can reach up to 64 Gbps. The details of the backend system are introduced in Section 2.4. The block diagram of receiver and backend of the KPC are illustrated in Figure 13.

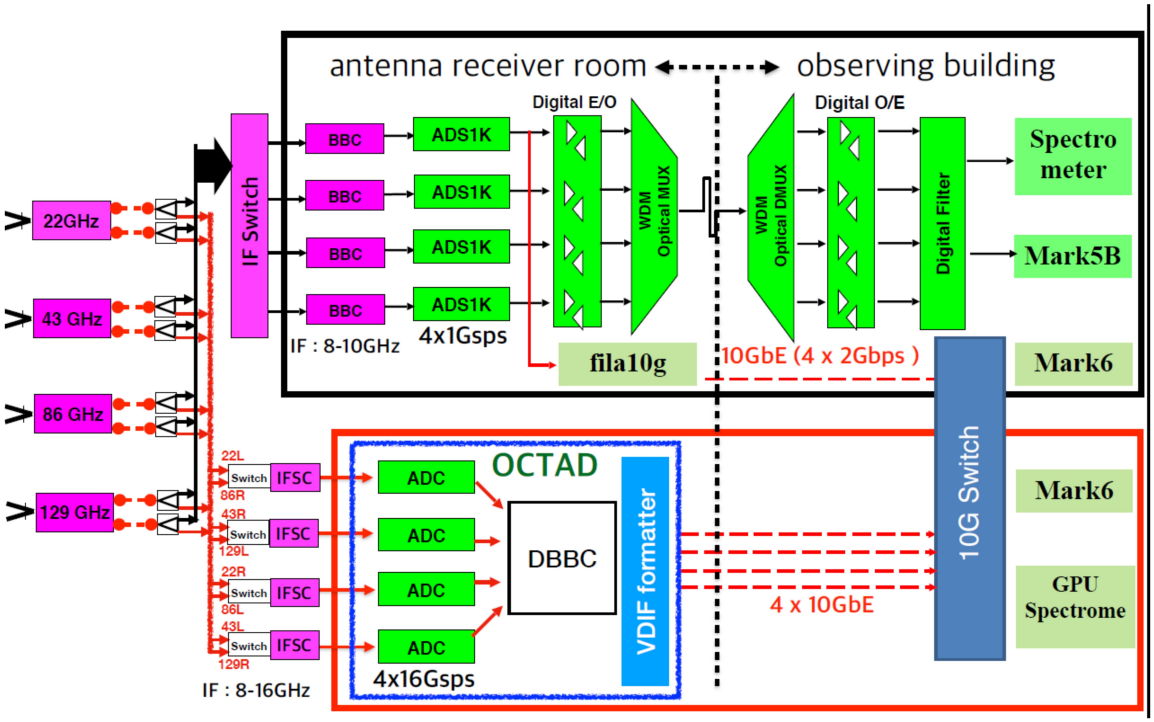

Figure 12: KVN signal flows including a new wide-band sampler OCTAD (from 2020).

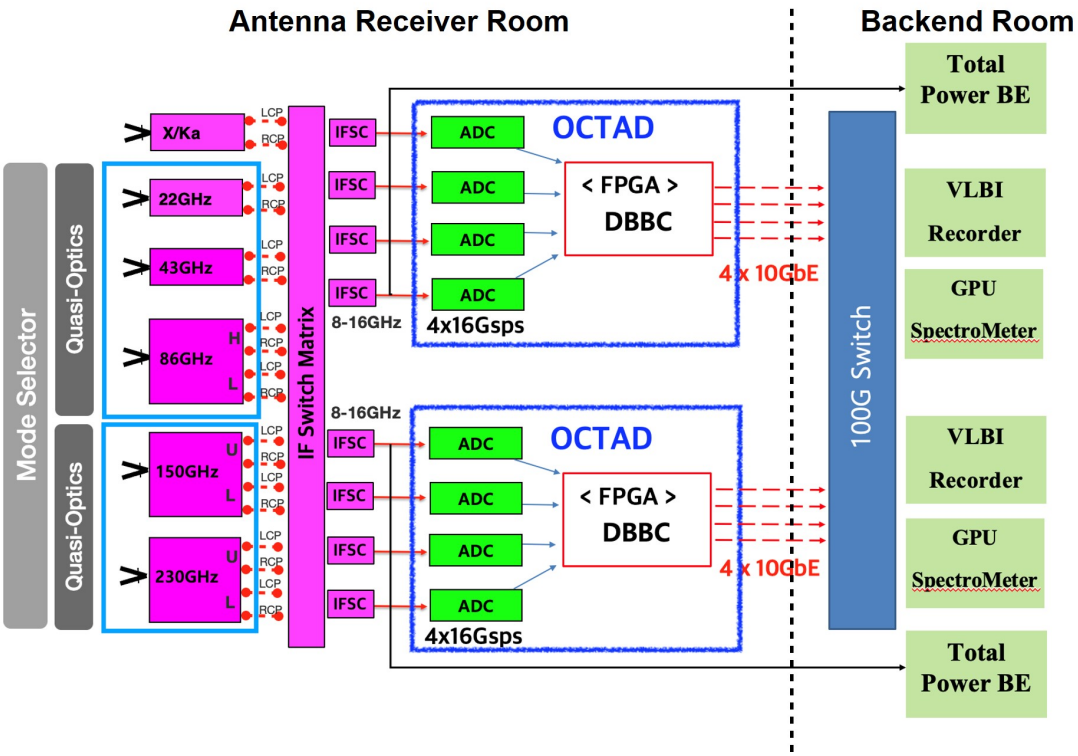

Figure 13: Block diagram of receiver and backend of the KPC.

2.3.3 Frequency range

The instantaneous bandwidth of the 1st IF of each receiver is limited to 8 GHz by the band-pass filter. Table 8 shows the frequency range of each receiver. The Q and W bands are divided into two frequency ranges. The low (high) frequency ranges of the Q band receiver are from 35 (42) to 42 (50) GHz. The low (high) frequency ranges of the W band receiver are from 85 (100) to 100 (116) GHz. Low- and high-frequency bands of the same polarization cannot be observed at the same time. Note that the D band receiver has 2 GHz IF bandwidth. The KPC with CTR system has slightly different frequency bands than the original KVN receivers. In the future, all original KVN receivers will be replaced with the CTR system.

2.3.4 Receiver noise temperature

Every frequency band has a receiver noise temperature that ranges from roughly 50 to 80 K. These values are similar for all bands. The loss of quasi-optics does not reduce the efficiency of the antenna aperture since the calibration chopper is placed before the quasi-optics; rather, it raises the temperature of the receiver noise. As a result, 40-–50 K are added to the noise temperatures to account for the quasi-optics losses.

Table 8: Frequency range of the KVN receiver

Band	Frequency range (GHz)	Telescope
C/X	6 – 9	KUS, KPC (in prep.)
Ka	28 – 34	KPC (in prep.)
K	18 – 26	KYS, KUS, KTN, KPC–CTR
Q-low	35 – 43	KYS, KUS, KTN, KPC–CTR
Q-high	42 – 50	KYS, KUS, KTN, KPC–CTR
W-low	85 – 100	KYS, KUS, KTN
W-high	100 – 116	KYS, KUS, KTN
W-low	80 – 98	KPC–CTR
W-high	98 – 116	KPC–CTR
D	125 – 142	KYS, KUS, KTN
D-wide	125 – 170	KPC (in prep.)
sub-mm	210 – 275	KPC (in prep.)

2.3.5 System temperatures with wide-band frequencies

Wide-band observations are now possible with the KVN thanks to the integration of the GPU spectrometer and a new backend (OCTAD). In this regard, we evaluated the system temperatures over all wide-band frequency ranges, and the results are presented in Table 9 and Figure 14. With regard to the KPC, the test observations for the wide-band mode are still underway.

2.4 Backend/Digital Process

The KVN backend comprises a (wide-band) sampler that converts the IF signal from the receiver into a digital signal and a (wide-band) high-speed recorder that transfers the signal from the sampler to the hard disk. The KVN currently employs two modes: DAS system and OCTAD, a wide-band VLBI sampler.

2.4.1 Digital filter mode in DAS

The digital filter bank (DFB) is configurable to various modes according to the required number of streams and bandwidths. The DFB enables us to select in frequency domain 16 data streams of 16 MHz bandwidth from 4 streams of 512 MHz bandwidth. The corresponding data rate of the 16×16 MHz stream is 1024 Mbps, which corresponds to the maximum input data rate of the Mark5b recorder. Combining more than one stream, the DFB can produce streams with wider bandwidth such as 8×32 MHz, 4×64 MHz, 2×128 MHz, and 1×256 MHz (see Table 10).

A center frequency of a data stream is given by BW$\cdot$(0.5 + N), where BW and N represent a bandwidth of data stream and integer number, respectively. If N is an even number, the data stream is the upper sideband. Otherwise, the data stream is in the lower sideband.

Table 9: System temperatures ($T_{\rm sys}$) using wide-band frequencies

Site	Band	Freq. range (GHz)	$T_{\rm sys}$ (K)	El. (degree)	Date
KYS	K	18 – 26	82 – 98	45 – 49	Jan. 17, 2023
	Q-low	35 – 42	60 – 112	51 – 52	Jan. 17, 2023
	Q-high	42 – 50	91 – 140	45 – 48	Jan. 17, 2023
	W-low	85 – 100	147 – 191	59 – 65	Jan. 27, 2023
	W-high	100 – 116	131 – 255	40 – 43	Feb. 01, 2023
	D	125 – 142	139 – 180	35 – 51	Jan. 27, 2023
KUS	K	18 – 26	71 – 91	55 – 56	Feb. 08, 2023
	Q-low	35 – 42	51 – 118	51 – 52	Feb. 08, 2023
	Q-high	42 – 50	85 – 156	46 – 48	Feb. 08, 2023
	W-low	85 – 100	153 – 203	48 – 61	Feb. 08, 2023
	W-high	100 – 116	150 – 315	43 – 61	Feb. 10, 2023
	D	125 – 142	145 – 279	36 – 46	Feb. 08, 2023
KTN	K	18 – 26	71 – 77	59 – 62	Feb. 20, 2023
	Q-low	35 – 42	58 – 85	49 – 58	Feb. 20, 2023
	Q-high	42 – 50	79 – 121	58 – 59	Feb. 20, 2023
	W-low	85 – 100	114 – 159	59 – 65	Feb. 20, 2023
	W-high	100 – 116	101 – 142	57 – 63	Feb. 21, 2023
	D	125 – 142	121 – 163	37 – 48	Feb. 24, 2023
KPC	K	21 – 25	53 – 79	30 – 64	Feb. 01, 2024
	Q	43 – 47	96 – 160	30 – 64	Feb. 01, 2024
	W	86 – 90	228 – 286	30 – 64	Feb. 01, 2024

Therefore, adjacent data streams have opposite sidebands. The center frequency cannot exceed 512 MHz.

2.4.2 Signal processing mode of OCTAD

The OCTAD provides various configurable modes. It enables us to select in the frequency domain a maximum of 16 data streams from 4 streams of 8192 MHz bandwidth. The maxi-

Table 10: KVN digital filter mode

Bandwidth (MHz)	Number of streams
16	16
32	8
64	4
128	2
256	1

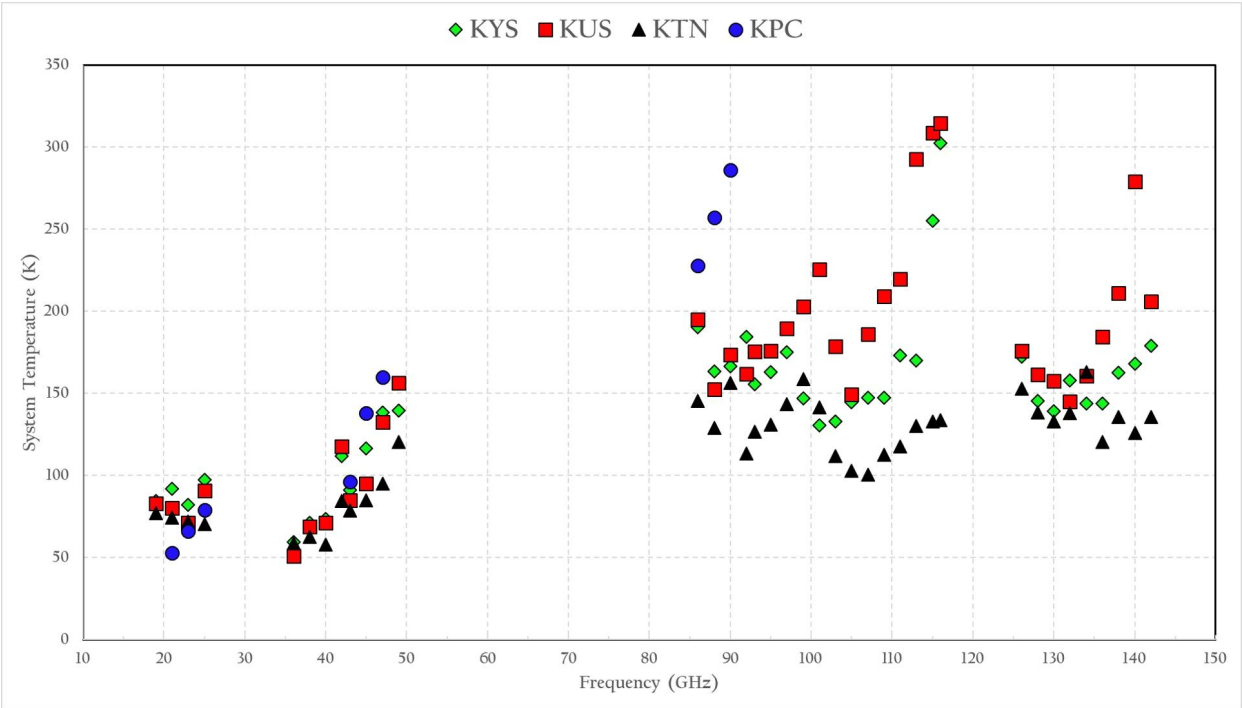

Figure 14: System temperature changes with all wide-band frequencies of 3 KVN telescopes.

mum output rate is 32 Gbps (4×8 Gbps) of which the net bandwidth is 8 GHz (4×2 GHz bandwidth). The possible mode of OCTAD is listed in Table 11. There is no restriction on the frequency step and the order of sideband in the OCTAD digital down-converter, unlike the digital filter.

Meanwhile, as mentioned above, the KPC is outfitted with 2 OCTADs, while the original KVN telescopes were equipped 1 DAS and 1 OCTAD systems. As a result, the maximum output rate of the KPC reach 64 Gbps, which corresponds to an 8 GHz bandwidth for 2-bit sampled data. Notably, this enhancement aligns the KPC with the observing mode specifications (2 GHz $\times$ 2 IF $\times$ 2 pol.) of the Event Horizon Telescope (EHT). Only one OCTAD is currently available for the KPC, and the second OCTAD will be installed soon.

Table 11: KVN OCTAD mode

Bandwidth (MHz)	Max. Number of streams	Total data rate (Gbps)
16	16	1
32	16	2
64	16	4
128	16	8
256	16	16
512	16	32
1024	8	32
2048	4	32

2.4.3 Recorders

KVN station has two recording systems, Mark5b and Mark6.

Mark5b and Mark6 are hard disk recording systems developed at Haystack Observatory, USA. The maximum data rate of Mark5b and Mark6 systems is 1 Gbps and 16 Gbps, respectively. For more details, see Haystack-memo-MK5b and Haystack-memo-MK6. At KVN stations, the Mark5b records the output data stream of a digital filter. Refer to section 2.3.2 for data stream connection and section 2.4.1 for available bandwidth and number of channels of 1 Gbps data stream.

Mark6 records output data streams of four samplers via Fila10G. The Fila10G converts four VSI streams from four samplers into VDIF (VLBI Data Interchange Format) data and sends them to the Mark6 on a 10 GbE network connection. There is no digital filtering function in the Fila10G. Therefore, single IF of Mark6 data of the KVN always has 512 MHz bandwidth. 2 Gbps (1 IF $\times$ 512 MHz), 4 Gbps (2 IF $\times$ 512 MHz) and 8 Gbps (4 IF $\times$ 512 MHz) modes are available in the KVN using the Mark6. The OCTAD VDIF output can be recorded by Mark6. For OCTAD 32 Gbps mode, all two Mark6 should be employed only for the OCTAD output. We cannot record Fila10G output. Therefore, we can observe no more than four IF signals among eight in OCTAD 32 Gbps mode.

From 2022, we adopted **Flexbuff**, a system for recording VLBI data at super high speeds, developed by JIVE and proven for its performance and reliability by EVN and other networks (Figure 15). The Flexbuff system consists of a single host-based hardware that integrates more than 32 HDD arrays and storage servers to store high volume and high bandwidth files, and software that supports data recording at 32 Gbps. In the absence of dedicated hardware to produce the Flexbuff, the KVN chose PCI-E 4.0, 3rd generation CPU to handle the four 8 Gbps streams output from the OCTAD in real time. The Flexbuff platform of the "Supermicro" model has been installed at all KVN sites, including the KPC site. Additionally, **jive5ab**, a copy manager software designed for recording and transmitting VLBI data, based on the Linux OS "Rocky" has also been installed.

2.4.4 Spectrometers for Single-dish observation

- **Digital spectrometer**
  The VSI output data from the digital filter with an aggregation rate of 1024 MHz (256 MHz bandwidth) is processed using an FX-type digital spectrometer (DSM). The DSM is capable of processing 4 VSI streams that are sent from samplers via optical transmission. It processes data with a bandwidth of 4×512 MHz. It is capable of generating both cross- and auto-power spectrum data. For the purpose of observing polarization, cross-power spectrum measurements are employed. In all modes, the total number of FFT points accessible is set at 4096 channels per stream.

- **GPU Spectrometer**
  The GPU (Graphics Processing Unit) spectrometer processes VDIF data streams from OCTAD to create a power spectrum using FFT computations. The modalities that are accessible vary depending on the performance of the GPU cards and the host server of the GPU spectrometer in each station. Table 12 provides a summary of them. Because of its considerable flexibility, the GPU spectrometer can accommodate

Figure 15: Front view of the two Flexbuff units at KPC. 24 disks are mounted for one Flexbuff.

various numbers of FFT points. In a 32 MHz stream, we can obtain at least 4096 FFT points. As with a digital spectrometer, the GPU spectrometer can generate both auto- and cross-power spectrum data. However, because it is still under testing and evaluation, the polarization observation mode employing the GPU spectrometer's cross-power spectrum output is not currently available.

2.4.5 Correlator

- **Daejeon Correlator in KJCC**
  KJCC(Korea-Japan Correlation Center) gathers the raw VLBI observation data from each site of KVN, VERA/JVN, and CVN, and performs the correlation process with two VLBI correlators. The first one, Daejeon Correlator, is one of the fastest VLBI correlators in the world and is used for processing the KaVA and EAVN observations mainly. It is capable to correlate the data streams of max. 8 Gbps for max. 16 stations in one pass, to produce the correlated output of 8192 spectral points for each sub-bands. The number of spectral points is reduced to 128 for continuum, 512 for line observation after the correlation process by channel integration.

  For the final correlation output, the default accumulation time is 1.6384 seconds and the final frequency resolutions are 16–128 MHz for continuum observations, and 16–512 MHz for line observations in default.

Table 12: Available mode of the GPU spectrometer

Bandwidth (MHz)	Number of streams	Total data rate (Gbps)
32	16	2
64	16	4
128	16	8
256	8	8
512	4	8
1024	2	8
2048	1	8

The KJCC is currently able to support the following correlation modes (see Table 13).

Table 13: Correlation mode of the KJCC

Obs. Mode	Total Data Rate	Bandwidth /sub-band	# of sub-bands	Minimum Accum. Time	# of Freq. Channels /sub-band
C5	1024 Mbps	16 MHz	16	1.6384 sec	8192
C4	1024 Mbps	32 MHz	8	0.8192 sec	8192
C3	1024 Mbps	64 MHz	4	0.4096 sec	8192
C2	1024 Mbps	128 MHz	2	0.2048 sec	8192
C1	1024 Mbps	256 MHz	1	0.1024 sec	8192
W1	2048 Mbps	512 MHz	1	0.0512 sec	8192
W2	4096 Mbps	512 MHz	2	0.0512 sec	8192
W4	8192 Mbps	512 MHz	4	0.0512 sec	8192

The KJCC supports the following number of frequency channels for preparing FITS file.

- Basic output channel of correlator: 8192 frequency channel
- Continuum: 128 frequency channel (64 channels integrated in post-correlation)
- Spectral line: 512 frequency channel (16 channels integrated in post-correlation)

Correlation processing will take about 1 week to prepare the first version of FITS after the data arrives from the last station. However, the KJCC team will do their best to make correlation results available as quickly as possible to deliver the FITS file to PI. For more details, please see the homepage KJCC.

- **Software Correlator, DiFX**
  The second one, DiFX (Distributed FX-style) software correlator (see Deller et al. (2007 [6], 2011 [7]), is the world-famous software correlator and is used for processing the KVN observations. It provides quite flexible correlation modes. You can request the accumulation time and the frequency resolution appropriate for your science purpose.

A dedicated computing cluster named "Coma" for software correlation was installed. It is composed of one master and eight computing nodes. The master node has 128 GB of memory and two Intel Xeon E5−2667 v3 processors. Each of the processors has eight cores. Each computing node has 128 GB of memory and two Intel Xeon E5−2698 v4 processors. Each of the processors has 20 cores. The master and computer nodes are connected with 100 Gbps Infiniband and 1 Gbps Ethernet. The Infiniband connection is for parallel computation and storage, and the Ethernet connection is for management. OpenHPC has been used to deploy and manage the Coma cluster. A dedicated Lustre file system for the software correlation provides about 3 petabytes. It is connected to the master and each computing node through 100 Gbps Infiniband.

Observation data saved in Mark5b or Mar6 at each KVN site is transported to the Luster file system through the KREONET using GridFTP. The master node has an additional 100 Gbps Ethernet connection to the KREONET. The KYS site is connected to the KREONET using 40 Gbps Ethernet, and the KUS and KTN sites are connected using 10 Gbps. Figure 16 shows the Coma computing cluster and the Lustre file system. Technical details of the software correlator are described in the homepage DiFX.

- **FITS delivery**
  Correlations will be done using either the DiFX or the Daejeon correlator. The KJCC will deliver the FITS file to PI by using an FTP server or mobile disk.

  – When the correlation is completed, the FITS file will be prepared by post processing, and then the KJCC will announce the completion of the correlation processing to the PI by e-mail. In the e-mail, PI will be able to get the FITS file via a temporary URL link.

  – The PI should download the FITS file as soon as possible and check the FITS file using his or her preferred analysis tool. And then the PI should give his response to KJCC with "Success" (data quality is good) or "Fail" (download fail, bad FITS file, data quality is bad, etc.). Especially in the case of the "Fail" opinion, please send the error message to the KJCC, Your quick response for the FITS will be helpful for the KJCC to solve the problem as soon as possible.

  – The KJCC would like to receive PI's response within 2 weeks after announcing the email. If there is no response within 4 weeks, the KJCC determines that the PI's response is regarded as "success".

  – In case of "Fail", according to the fail type, the KJCC will conduct the URL check, file reconstruction, or re-correlation, and then an announcement will be sent again to PI via e-mail.

  – In the case of "Success", correlation processing for that observation will be closed (at that time, the download link in the temporary URL will be unavailable), and the tapes or disk modules will be included in the release pool for recycling.

  – The FITS file provided to PI will be stored separately at the observation data archive. The PI should analyze, perform the research, and publish the paper within some period of time (in general, 18 months). After 18 months, the FITS

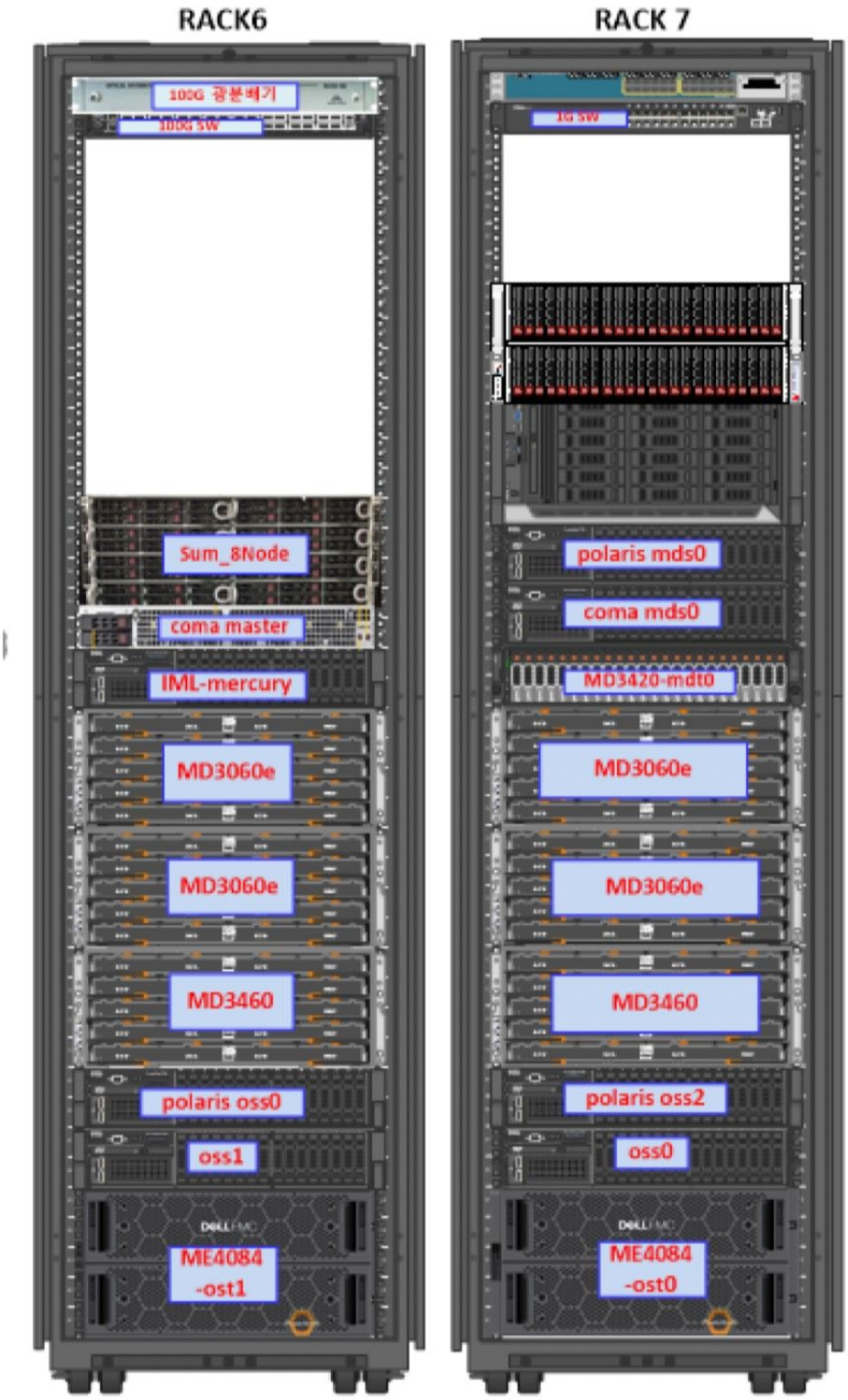

Figure 16: A computing cluster and Lustre file system dedicated for the software correlation of the KVN.

file stored in the archive system will be opened to the public, who will need to do their research using that FITS according to the procedures.

- **Archiving policy**
  The KJCC organizes the archiving policy for observation data, CODA, and FITS files as below.
  - All VLBI data obtained with the KVN are accessible for collaborative purposes and will be utilized solely by the PI without external sharing until 18 months post-observation. After this exclusivity period, all data will be stored on KASI's dedicated servers and made publicly available through the Science Data Portal (http://data.kasi.re.kr, see Figure 17).
  - CODA: If correlated data is used for astrometry or geodesy, it is permanently stored at the CODA server. Otherwise, the correlated raw data and CODA file system will be deleted after receiving the response from PI.
  - FITS: it is permanently archived at the Archiving server.

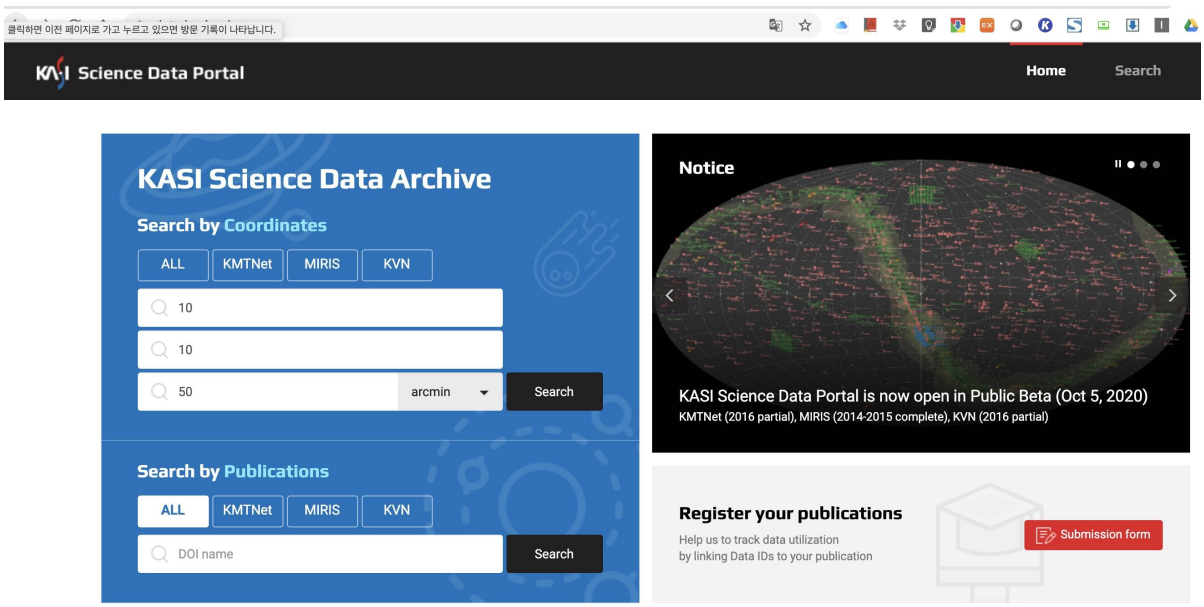

Figure 17: Initial screen of the KASI Science Data Portal

2.5 Calibration for VLBI observations

System temperatures in Kelvin ($T_{\rm sys}$) are measured during observations at KVN stations once every user-specified interval (default 10 sec) to calibrate amplitude variation in time due mainly to atmospheric fluctuation. The measured $T_{\rm sys}$ is a sum of three temperatures: the receiver temperature, the spillover temperature, and the contribution of the atmosphere as described in Petrov et al. (2012) [8]. These $T_{\rm sys}$ values can be converted to SEFD (System

Equivalent Flux Density) by dividing by the KVN antenna gains in K/Jy. The elevation dependence of the antenna gains is also corrected based on the normalized gain curves with lease-squared-fitted second-order polynomials as derived in Lee et al. (2011) [9].

Additional amplitude correction for the atmospheric opacity above an antenna is performed by conducting a sky tipping curve analysis according to the method described in Mangum (2000). In practice, the system temperatures ($T^*_{\rm sys}$) corrected for the atmospheric opacity are estimated based on the sky tipping curve measurements once every user-specified interval (default before and after an experiment). Further corrections are made to the KVN observations taken with 2-bit (4-level) sampling, for the systematic effects of the non-optimal setting of the quantizer voltage thresholds.

The amplitude calibrations with the KVN are accurate to 15 % or better at 22 and 43 GHz. However, it is recommended to observe a few amplitude calibrators during the scheduled observation time, allowing for (a) the assessment of the relative gains of KVN antennas and gain differences between IF-bands at each station, and (b) the confirmation of the correlation coefficient correction assuming that you have contemporaneous source flux densities obtained with other VLBI networks independent of the KVN observations.

2.6 KVN geodetic VLBI measurement

Obtaining accurate antenna positions is important in the VLBI system, especially for high precision astrometry. KVN antenna positions are regularly monitored using GPS and geodetic VLBI observations. The K-band geodesy VLBI program between KVN and VERA started in 2011. Current KVN antenna positions (see Figure 18) were obtained from the KaVA K-band geodesy on January 24, 2014. The typical 1-sigma errors of geodetic solutions are about 0.4 cm in the X, Y, and Z directions. Based on 22-epoch KaVA K-band geodetic observations from September 2012 to December 2016, uncertainties of KVN antenna positions are $\sim$ 2.38 cm at KYS, $\sim$ 2.55 cm at KUS, and $\sim$ 1.58 cm at KTN.

The accurate positions of the KVN antennas were recently derived from IVP measurements using GNSS. These are described in Section 2.1.3.

3 Observing proposal

3.1 Observing mode

3.1.1 Multi-frequency observation

Simultaneous multi-frequency observation is a unique capability of the KVN, with which we can calibrate out the short-term phase fluctuations at higher frequency data by referencing the phase solution obtained from lower frequency data. This phase referencing technique allows us to integrate the data for a time scale much longer than the coherent time scale of atmospheric phase fluctuation and so to observe weak sources at mm-wavelength efficiently. For multi-frequency observations, we can select no more than 4 IFs among 8 IF signals (= 4 receivers $\times$ 2 polarizations).

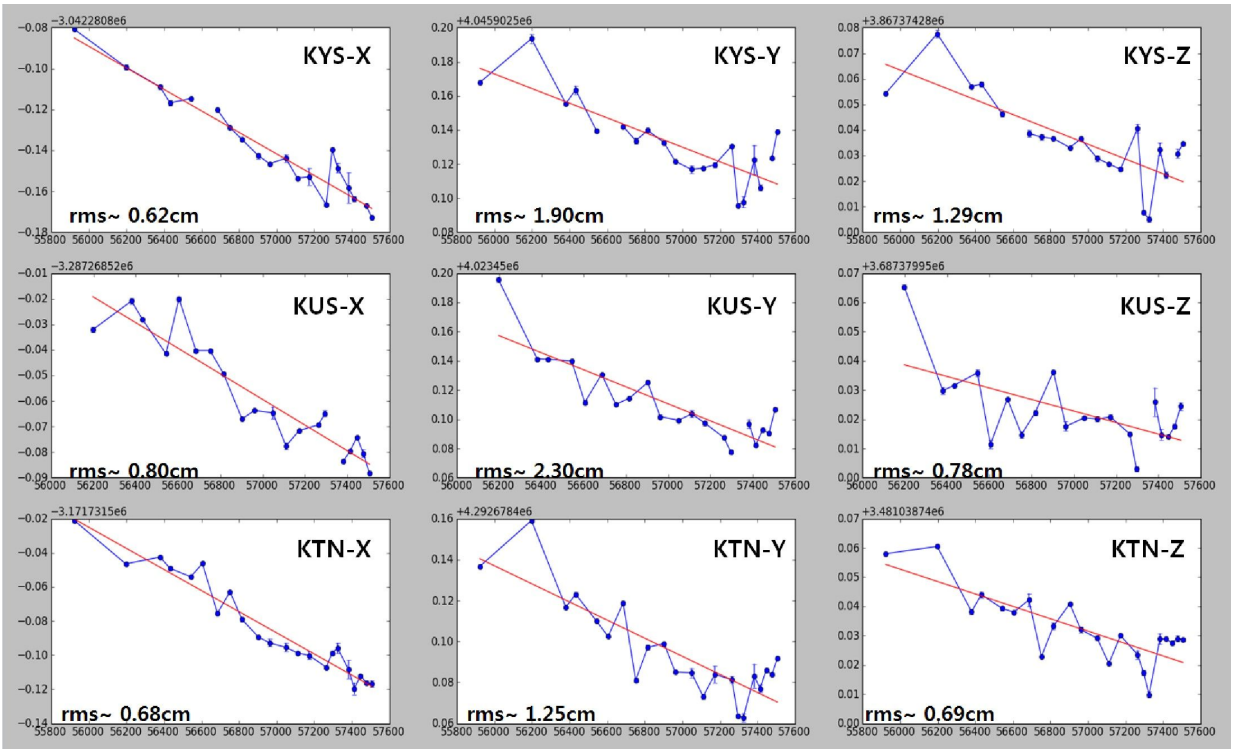

Figure 18: The trend of KVN antenna positions (IVP) in the ITRF 2014 coordinate system. The x and y axes are MJD and X, Y, and Z in meters. The linear fitting is applied to the measurements, shown as red line, and its deviation is also presented in each axis as "rms".

3.1.2 Fast position switching observation

The slewing speed and acceleration rate of the KVN antenna are 3 °/sec and 3 °/sec^2, respectively. Due to this high speed and acceleration rate, the KVN antenna can switch its pointing from target to calibrator in a short period of time.

3.1.3 Recording rate

2 Gbps (1×512 MHz), 4 Gbps (2×512 MHz), 8 Gbps (4×512 MHz) modes, which use fila10G and Mark6 recorders, have been fully evaluated in 2017. These modes are currently available for common use observations. For multi-frequency observations, we can select 1, 2, or 4 IFs among 8 IF signals (= 4 receivers × 2 polarizations). Furthermore, observations in 16 Gbps and 32 Gbps modes are now available following the installation of the high-speed recorder FlexBuff and the VLBI sampler OCTAD. These are explained with additional detail in Section 2.4 and are further addressed below.

- 16 Gbps mode
  - KYS, KUS, KTN: OCTAD (*8 Gbps) + 4 ADS1K + fila10G (8 Gbps: 512 MHz × 4 CH)
    *8 Gbps: 128 MHz × 16 CH, 256 MHz × 8 CH, 512 MHz × 4 CH

- KPC: OCTAD1: 8 Gbps, OCTAD2: 512 MHz × 4 CH (4 Gbps)

- 32 Gbps mode (for Flexbuff)
  - 2048 MHz × 4 CH, 1024 MHz × 8 CH, 512 MHz × 16 CH

3.2 Angular resolution

Table 14 shows the maximum lengths (B) of the KVN baselines in km and the corresponding resolutions ($\theta_{\rm HPBW}$) in milli-arcsecond (mas), which is estimated as $\theta_{\rm HPBW}$ (mas) $\sim 20627 \cdot \lambda$(mm)/B(km).

Table 14: Angular resolutions at each KVN baseline and frequency

Baseline	B (km)	$\theta_{\rm HPBW}$ (mas)			
		22 GHz	43 GHz	86 GHz	129 GHz
KYS–KUS	305.0	9.1	4.7	2.4	1.6
KUS–KTN	358.8	7.8	4.0	2.0	1.3
KTN–KYS	478.0	5.8	3.0	1.5	1.0
KPC–KYS	133.1	20.9	10.8	5.4	3.6
KUS–KPC	232.6	12.0	6.2	3.1	2.0
KTN–KPC	505.8	5.5	2.9	1.4	0.9

3.3 Baseline sensitivity

Table 15 shows sensitivities of the KVN baselines as follow: (1) frequency band, (2) nominal frequency range of KVN receivers, (3) system temperature, (4) typical KVN system-equivalent-flux-density at zenith, (5) antenna gain at the optimal elevation, (6) typical KVN baseline sensitivity for the aggregated recorded data rate of 1024 Mbps, the integration time of 100 sec (K-band), 60 sec (Q-band), and 30 sec (W/D-band), and the bandwidth of 256 MHz, and (7) typical KVN 3-baseline image sensitivity for the on-source integration time of 8 hr.

Table 15: Baseline sensitivity of the KVN

Freq. band	Freq. range (GHz)	$T_{\rm sys}$ (K)	SEFD (mJy)	Gain (K/Jy)	ΔS (mJy)	ΔI (mJy/beam)
(1)	(2)	(3)	(4)	(5)	(6)	(7)
K	21.25–23.25	100	1129	0.089	12	0.2
Q	43.11–44.11	150	1715	0.087	18	0.3
W	85–95	200	2073	0.072	29	0.6
D	125–142	250	3041	0.049	54	1.0

3.4 System temperature

Figure 19 shows seasonal variation of system temperature at each KVN site. The zenith system temperatures corrected for atmospheric attenuation at K-, Q-, W-, and D-bands are presented by four panels from top to bottom, respectively.

3.5 Astrometric observation

Numerous factors (antenna locations, calibrators, timetable, etc.) need to be properly examined and planned to produce accurate astrometric observations. Astrometric VLBI observations using the KVN are not supported at this time. To evaluate the feasibility, we got underway astrometric AGN/Maser test observations; the outcomes will be provided the following year. Please get in touch with us if you wish to make an astrometric observation.

4 Observation and Data Reduction

4.1 Preparation of observation and correlation

4.1.1 General information

For the accepted proposals, the users have to prepare the observing schedule file before the observation. The observer who is not familiar with the KVN system is recommended to consult contact persons of the KVN group to prepare schedules, especially for some observations such as phase referencing, polarimetry, and/or spectral line, etc. The detailed information about observation planning and scheduling can be downloaded from the KVN homepage[2].

4.1.2 Observation

All KVN experiments should be scheduled using the VEX (VLBI experiment) file. You can either edit and modify the KVN VEX example files or use the VLBA scheduling program SCHED[3]. It is recommended to use SCHED for your scheduling because SCHED provides useful information and many aspects of planning VLBI observations, and you can also avoid many mistakes arising from editing the VEX manually. The user needs to submit the VEX or key files two weeks before the observation. KVN AOC staff will check your schedule and proceed with the observations.

4.1.3 Correlation

Following the observation, the Daejeon correlator or DiFX correlator will perform the correlation procedure in accordance with the parameters that were provided. In order to release and recycle the disk modules and storage used for observation, the user is required to review the correlated data and report if the correlation was correctly performed. If there are any issues, re-correlation may be required. The raw data disk modules utilized for the

[2] https://radio.kasi.re.kr/kvn/user_support.php
[3] http://www.aoc.nrao.edu/~cwalker/sched/sched.html

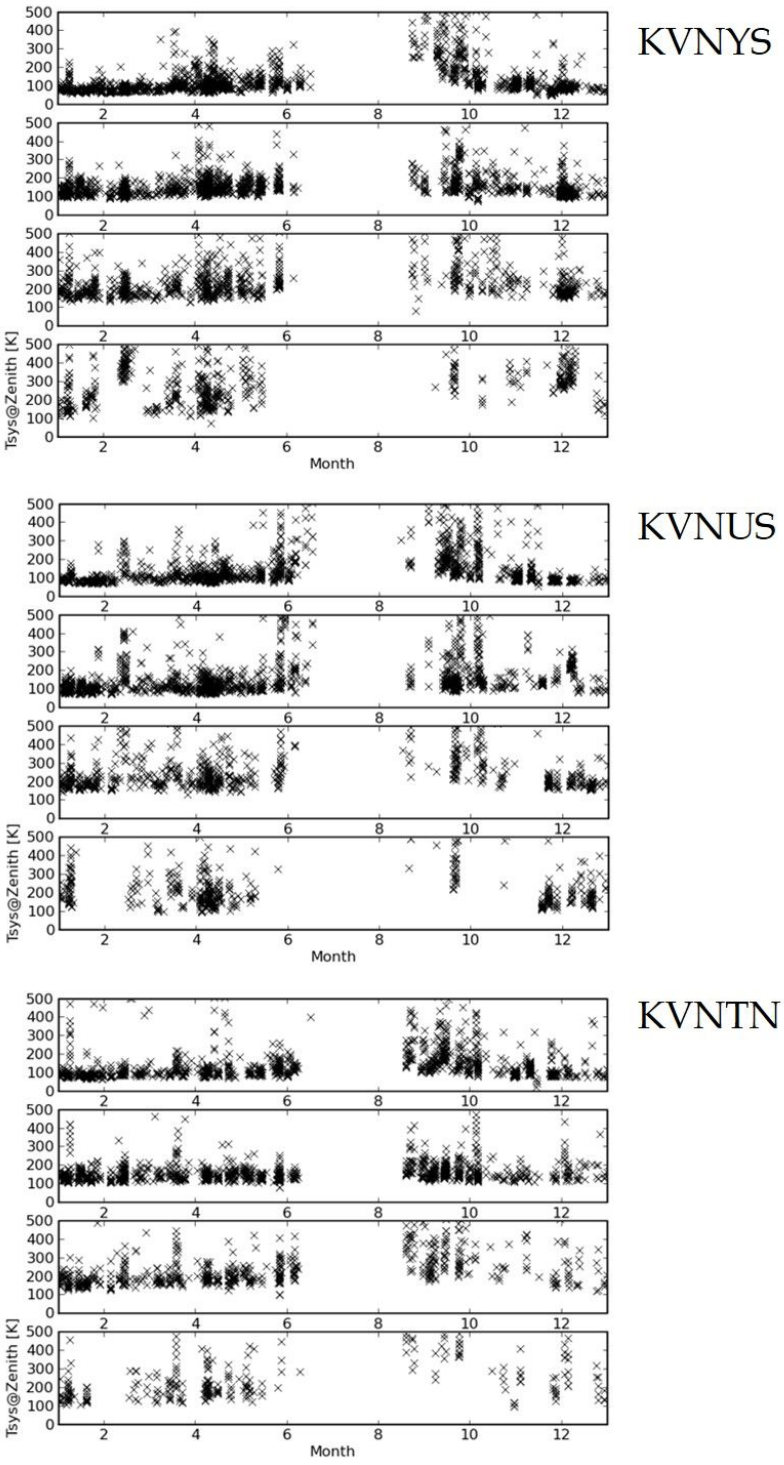

Figure 19: System temperatures of each KVN telescope

observations will, in principle, be discarded two months after the correlation. Please see the correlation status report for further details.

4.2 Data reduction

4.2.1 VLBI data reduction with AIPS

Here we introduce a very brief way of reducing VLBI data with KVN (or EAVN). For more detail, please have a look at the data reduction manual[4]. Figure 19 shows one of the procedures for reducing the KVN (or EAVN) observations.

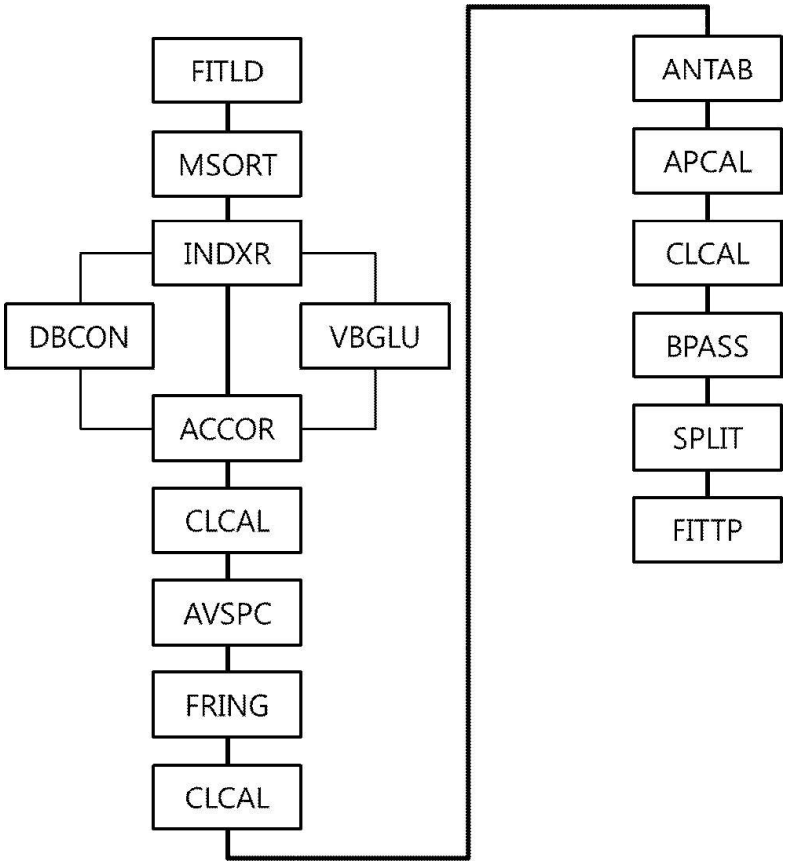

Figure 20: Data reduction flow chart with AIPS

5 Further information

Contact address It is possible for users to contact any staff member of the KVN by email (see Table 16). The official website[5] also provides various types of information.

[4] https://radio.kasi.re.kr/eavn/user_support.php
[5] http://kvn.kasi.re.kr

Table 16: Contact information

E-mail	Subject
kvnprop@kasi.re.kr	Proposal submission and informing its result
kvnobs@kasi.re.kr	Observing schedule submission, observation-related requests and questions for the accepted proposal only
kjcc@kasi.re.kr	Correlated data distribution and correlation-related requests
kvnhelp@kasi.re.kr	General questions including scheduling, observations, systems, and so on (regardless of the proposal acceptance)

References

[1] S.-S. Lee, L. Petrov, D.-Y. Byun, J. Kim, T. Jung, M.-G. Song, C. S. Oh, D.-G. Roh, D.-H. Je, S.-O. Wi, B. W. Sohn, S.-J. Oh, K.-T. Kim, J.-H. Yeom, M.-H. Chung, J. Kang, S.-T. Han, J.-W. Lee, B. G. Kim, H. Chung, H.-G. Kim, H. Ryoung Kim, Y.-W. Kang, and S.-H. Cho, "Early Science with the Korean VLBI Network: Evaluation of System Performance," The Astronomical Journal, vol. 147, p. 77, Apr. 2014.

[2] I. de Pater, R. J. Sault, M. H. Wong, L. N. Fletcher, D. DeBoer, and B. Butler, "Jupiter's ammonia distribution derived from VLA maps at 3-37 GHz," Icarus, vol. 322, pp. 168–191, Apr. 2019.

[3] M. Maris, E. Romelli, M. Tomasi, A. Gregorio, M. Sandri, S. Galeotta, D. Tavagnacco, M. Frailis, G. Maggio, and A. Zacchei, "Revised planet brightness temperatures using the Planck/LFI 2018 data release," Astronomy and Astrophysics, vol. 647, p. A104, Mar. 2021.

[4] S.-T. Han, J.-W. Lee, J. Kang, D.-H. Je, M.-H. Chung, S.-O. Wi, T. Sasao, and R. Wylde, "Millimeter-wave Receiver Optics for Korean VLBI Network," International Journal of Infrared and Millimeter Waves, vol. 29, pp. 69–78, Jan. 2008.

[5] S.-T. Han, J.-W. Lee, J. Kang, C.-S. Oh, D.-Y. Byun, D.-H. Je, M.-H. Chung, S.-O. Wi, M. Song, Y.-W. Kang, S.-S. Lee, S.-Y. Kim, T. Sasao, P. F. Goldsmith, and R. Wylde, "Korean VLBI Network Receiver Optics for Simultaneous Multifrequency Observation: Evaluation," Publications of the Astronomical Society of the Pacific, vol. 125, p. 539, May 2013.

[6] A. T. Deller, S. J. Tingay, M. Bailes, and C. West, "DiFX: A Software Correlator for Very Long Baseline Interferometry Using Multiprocessor Computing Environments," , vol. 119, pp. 318–336, Mar. 2007.

[7] A. T. Deller, W. F. Brisken, C. J. Phillips, J. Morgan, W. Alef, R. Cappallo, E. Middelberg, J. Romney, H. Rottmann, S. J. Tingay, and R. Wayth, "DiFX-2: A More Flexible, Efficient, Robust, and Powerful Software Correlator," , vol. 123, p. 275, Mar. 2011.

[8] L. Petrov, S.-S. Lee, J. Kim, T. Jung, J. Oh, B. W. Sohn, D.-Y. Byun, M.-H. Chung, D.-H. Je, S.-O. Wi, M.-G. Song, J. Kang, S.-T. Han, J.-W. Lee, B. G. Kim, H. Chung,

and H.-G. Kim, "Early Science with the Korean VLBI Network: The QCAL-1 43 GHz Calibrator Survey," The Astronomical Journal, vol. 144, p. 150, Nov. 2012.

[9] S.-S. Lee, D.-Y. Byun, C. S. Oh, S.-T. Han, D.-H. Je, K.-T. Kim, S.-O. Wi, S.-H. Cho, B. W. Sohn, J. Kim, J. Lee, S.-J. Oh, M.-G. Song, J. Kang, M.-H. Chung, J. A. Lee, J. Oh, J.-H. Bae, S.-Y. Yun, J.-W. Lee, B. G. Kim, H. Chung, D.-G. Roh, C. H. Lee, H. G. Kim, H. Ryoung Kim, J.-H. Yeom, T. Kurayama, T. Jung, P. Park, M. J. Kim, D.-H. Yoon, and W.-J. Kim, "Single-Dish Performance of KVN 21 m Radio Telescopes: Simultaneous Observations at 22 and 43 GHz," Publications of the Astronomical Society of the Pacific, vol. 123, p. 1398, Dec. 2011.